BRNO UNIVERSITY OF TECHNOLOGY
VYSOKÉ UČENÍ TECHNICKÉ V BRNĚ

FACULTY OF ELECTRICAL ENGINEERING AND COMMUNICATION
FAKULTA ELEKTROTECHNIKY
A KOMUNIKAČNÍCH TECHNOLOGIÍ

DEPARTMENT OF RADIOENGINEERING
ÚSTAV RADIOELEKTRONIKY

CIRCULARLY POLARIZED ANTENNA ARRAY FOR ISM FREQUENCY BAND 24 GHZ
KRUHOVĚ POLARIZOVANÁ ANTÉNNÍ ŘADA PRO ISM PÁSMO 24 GHZ

BACHELOR'S THESIS
BAKALÁŘSKÁ PRÁCE

AUTHOR — Evans Liyambo
AUTOR PRÁCE

SUPERVISOR — prof. Dr. Ing. Zbyněk Raida
VEDOUCÍ PRÁCE

BRNO 2020

VYSOKÉ UČENÍ TECHNICKÉ V BRNĚ
FAKULTA ELEKTROTECHNIKY A KOMUNIKAČNÍCH TECHNOLOGIÍ

Bakalářská práce

bakalářský studijní program **Elektronika a komunikační technologie**

Ústav radioelektroniky

Student: Evans Liyambo ***ID:*** 203625
Ročník: 3 ***Akademický rok:*** 2019/20

NÁZEV TÉMATU:

Kruhově polarizovaná anténní řada pro ISM pásmo 24 GHz

POKYNY PRO VYPRACOVÁNÍ:

Seznamte se s konceptem kruhově polarizovaného anténního pole optimalizovaného pro pracovní kmitočet 45 GHz. Počítačovou simulací ověřte parametry jednoho prvku tohoto pole, porovnejte je s parametry konvenčního kruhově polarizovaného flíčku a rozhodněte, který element je vhodnější pro realizaci anténního pole 2x2 elementů. Svou volbu zdůvodněte.

Vybraný anténní prvek přepočítejte na pracovní kmitočet 24 GHz a na substrát zadaný vedoucím. Z přepočítaných anténních prvků vytvořte pole 4x4 elementů, pole optimalizujte a simulací ověřte jeho parametry.

DOPORUČENÁ LITERATURA:

[1] GAN, Zheng, Zhi-Hong TU, Ze-Ming XIE, Qing-Xin CHU a Yue YAO. Compact Wideband Circularly Polarized Microstrip Antenna Array for 45 GHz Application. IEEE Transactions on Antennas and Propagation [online]. 2018, 66(11), 6388-6392 [cit. 2019-05-12]. DOI: 10.1109/TAP.2018.2863243. ISSN 0018-926X. Dostupné z: https://ieeexplore.ieee.org/document/8425689/

[2] BALANIS, Constantine A. Antenna theory: analysis and design. 3rd ed. Hoboken, NJ: John Wiley, c2005. ISBN 0-471-66782-x.

Termín zadání: 3.2.2020 ***Termín odevzdání:*** 4.6.2020

Vedoucí práce: prof. Dr. Ing. Zbyněk Raida

prof. Ing. Tomáš Kratochvíl, Ph.D.
předseda rady studijního programu

Abstract

This thesis deals with the design and simulation of a circularly polarized antenna array optimized for operation in the 24 GHz ISM frequency band. A circularly polarized microstrip antenna element [1] designed for operation at the frequency 45 GHz, which was used in the antenna array design, was first verified for proper functionality in CST Microwave Studio, and its parameters were compared with a conventional patch antenna excited by a cross aperture. The microstrip antenna element was then redesigned to operate in the 24 GHz ISM frequency band for use in the antenna array design.

Keywords

Planar antenna array, circularly polarized antenna element, wideband antenna, CST Microwave Studio, cross-aperture coupled patch antenna.

Abstrakt

Tato bakalářská práce se zabývá návrhem a simulací kruhově polarizované anténní řady pro ISM pásmo 24 GHz. Kruhově polarizovaná mikropásková anténa [1] navržená pro práci na kmitočtu 45 GHz byla použita v návrhu anténní řady. Funkce použité antény byla ověřena v programu CST Microwave Studio a její parametry byly porovnány s konvenční flíčkovou anténou buzenou křížovou aperturou. Následně byla anténa modifikována tak, aby pracovala v ISM pásmu 24 GHz.

Klíčová slova

Planární anténní řada, kruhově polarizovaný anténní element, širokopásmová anténa, CST Microwave Studio, flíčková anténa buzená křížovou aperturou.

Rozšířený abstrakt

Cílem předložené bakalářské práce bylo seznámit se s konceptem kruhově polarizovaného anténního pole, optimalizovaného pro pracovní kmitočet 45 GHz. Prostřednictvím počítačové simulace měla být ověřena funkčnost daného anténního pole, a jeho struktura měla být následně přepočtena na pracovní kmitočet 24 GHz.

K ověření funkčnosti kruhově polarizované mikropáskové antény [1] navržené pro práci na kmitočtu 45 GHz byl využit program CST Microwave Studio a jeho řešič pro analýzu elektromagnetických struktur v časové oblasti. Všechny výsledky, které byly získány jako výstupy simulací, byly v souladu s výsledky publikovanými. Jedinou výjimkou byla šířka pásma osového poměru; výsledek 14,3% byl o 3% nižší, než bylo uvedeno v [1]. Z hlediska impedančního přizpůsobení anténa vykazovala širokopásmové chování; šířka pásma byla 25,1%.

Anténa publikovaná v [1] je konstrukčně relativně komplikovaná. Proto jsem se snažil ověřit, zda její komplikovaná geometrie přináší výhody v porovnání s konvenční flíčkovou anténou, která je buzena křížovou aperturou a je navržena na stejných substrátech. Rozměry konvenčního flíčku byly ve stejném kmitočtovém pásmu srovnatelné s [1], avšak jeho parametry byly přibližně třikrát menší. Pro přepočet do ISM pásma 24 GHz byla tedy vybrána publikovaná anténa.

Při návrhu antény určené pro pásmo 24 GHz jsem vyšel z parametrické analýzy antény. Ze získaných výsledků vyplynulo, že anténa vyzařuje kruhově polarizovanou vlnu hlavně díky dvěma poruchovým segmentům a pahýlům ve tvaru písmene L. Obě tyto struktury mají vliv nejen na osový poměr antény ale i na její rezonanční kmitočet a impedanční šířku pásma. Se zvyšováním hloubky poruchových segmentů se zlepšoval osový poměr, poklesl rezonanční kmitočet a zmenšila se impedanční šířka pásma. Zvýšení délky pahýlů mělo stejný vliv na osový poměr, ale zlepšil se činitel odrazu a šířka pásma zůstala téměř konstantní. Uvedené elementy byly proto využity k ladění osového poměru antény.

Kromě uvedených elementů (poruchových elementů a pahýlů) obsahuje anténa také dvě štěrbiny, které anténní flíček dělí na 4 segmenty, a dále prokovy kruhového průřezu, které propojují segmenty flíčku se zemní deskou. Podle analýzy se při zvyšování velikosti štěrbin v omezeném rozsahu (0,04 mm až 0,30 mm) zlepšuje impedanční šířka pásma a zhoršuje osový poměr. Prokovy by měly mít malý poloměr (v tomto případě v rozsahu 0,3 mm až 0,4 mm), a také vzdálenost mezi prokovy by měla být malá. S uvážením popsaných závislostí byla anténa optimalizována pro pracovní kmitočet 24 GHz. Její impedanční šířka pásma byla 14,2 %, šířka pásma osového poměru 1,4 % a maximální zisk na pracovním kmitočtu 8,8 dB.

Anténní prvek výše uvedených parametrů byl následně využit k sestavení anténního pole sestávajícího ze 2×2 anténních prvků na původních substrátech Rogers 5880 (horní substrát, $\varepsilon_r = 2{,}20$, $h = 0{,}787$ mm) a Rogers 4003 (dolní substrát, $\varepsilon_r = 3{,}55$, $h = 0{,}203$ mm). Impedanční šířka pásma tohoto anténního pole byla 24,6%, a maximální zisk dosahoval 13,9 dB. Anténní řada však dosáhla hodnoty osového poměru 3 dB pouze na pracovním kmitočtu 24 GHz.

Parametry pole by bylo možné zlepšit zmenšením vzdálenosti mezi jednotlivými prvky pole. Tuto redukci ale neumožňovala geometrie napájecího mikropáskového vedení. Proto byl dolní substrát Rogers 4003 (ε_r = 3,55, h = 0,203 mm) nahrazen substrátem ARLON CuClad217 s permitivitou ε_r = 2,17 a výškou h = 0,254 mm. Jako horní substrát byl využit ARLON CuClad217 se stejnou permitivitou a výškou h = 1,54 mm. Anténní řada pak dosáhla větší impedanční šířky pásma 33,5%, větší šířky pásma osového poměru 9,2% a maximálního zisku 13,5 dB. Vyzařovací charakteristika se však zhoršila.

Následně bylo navrženo anténní pole sestávající ze 4×4 elementů. K realizaci pole byly použity opět dostupné substráty ARLON CuClad. Navržené anténní pole vykazovalo impedanční šířku pásma 31,6% (pásmo kmitočtů 19,17 GHz až 26,75 GHz) a šířku osového poměru 14,2% (pásmo kmitočtů 22,96 GHz – 26,37 GHz). Zisk anténního pole byl vyšší než 16,5 dB v celém pásmu 19 GHz až 30 GHz; maximální hodnota zisku dosahovala úrovně 19,0 dB. Úroveň postranních laloků byla poměrně vysoká.

LIYAMBO, Evans. *Kruhově polarizovaná anténní řada pro ISM pásmo 24 GHz*. Brno, 2020. Dostupné také z: https://www.vutbr.cz/studenti/zav- prace/detail/126110. Bakalářská práce. Vysoké učení technické v Brně, Fakulta elektrotechniky a komunikačních technologií, Ústav radioelektroniky. Vedoucí práce Zbyněk Raida.

Prohlášení

Prohlašuji, že svou bakalářskou práci na téma Kruhově polarizovaná anténní řada pro ISM pásmo 24 GHz jsem vypracoval samostatně pod vedením vedoucího bakalářské práce a s použitím odborné literatury a dalších informačních zdrojů, které jsou všechny citovány v práci a uvedeny v seznamu literatury na konci práce.

Jako autor uvedené bakalářské práce dále prohlašuji, že v souvislosti s vytvořením této bakalářské práce jsem neporušil autorská práva třetích osob, zejména jsem nezasáhl nedovoleným způsobem do cizích autorských práv osobnostních a jsem si plně vědom následků porušení ustanovení § 11 a následujících autorského zákona č. 121/2000 Sb., včetně možných trestněprávních důsledků vyplývajících z ustanovení části druhé, hlavy VI. díl 4 Trestního zákoníku č. 40/2009 Sb.

V Brně dne 8. dubna 2020 .....

podpis autora

Acknowledgement

I would like to thank my supervisor Zbyněk Raida for his invaluable advice and support while working on this thesis.

Brno, the 8th of April 2020 .....

Author's signature

Content

List of symbols and abbreviations

Abbreviations:

CP	. . .	circularly polarized	

Symbols:

λ_d	. . .	wavelength in a dielectric	[m]
λ_0	. . .	wavelength in free space	[m]
v_0	. . .	speed of light in free space	[m/s]
f_r	. . .	resonance frequency	[Hz]
ε_r	. . .	relative permittivity	[-]
ε_{ef}	. . .	effective permittivity	[-]
W_p	. . .	width of the patch	[m]
L	. . .	length of the antenna	[m]
W	. . .	Width of the antenna	[m]
L_p	. . .	length of the patch	[m]
L_f	. . .	microstrip feed line length	[m]
W_f	. . .	microstrip feed line width	[m]
L_s	. . .	length of the aperture	[m]
W_s	. . .	width of the aperture	[m]
L_{stub}	. . .	length of the stub	[m]
ΔL	. . .	extension of the patch length	[m]
h	. . .	substrate height	[m]
Z_0	. . .	characteristic impedance	[Ω]
S11	. . .	reflection coefficient	[dB]
AR	. . .	axial ratio	[dB]
S	. . .	distance between metallic posts	[m]
G	. . .	space between the patches	[m]
P	. . .	dimensions of L-shaped branches	[m]
T	. . .	length of truncation	[m]
r	. . .	radius of the metallic posts	[m]

List of Figures

List of Tables

1. INTRODUCTION

At millimetre wave frequencies, signals become more prone to faster, harder and longer degradation due to atmospheric conditions. These atmospheric conditions can also cause a change in phase or rotation of the signal and attenuate it. Linear polarization is greatly affected by these conditions compared to circular polarization. For this reason, among others such as less sensitivity to orientation of both transmitting and receiving antennas and the advantage of multipath effects, circularly polarized antennas are given preference for use in wireless communication systems such as GPS, radar, satellite systems and in fifth-generation (5G) communications systems [1], [3], [4], [7].

In this thesis, a novel circularly polarized microstrip antenna element published in [1] designed to operate in the 45 GHz frequency band is redesigned and simulated and its results are verified with the published results. Its performance is then compared with that of a cross-aperture coupled patch antenna that was designed with the same substrates to operate in the same frequency band. The antenna element is then redesigned to operate in the 24 GHz ISM frequency band and used in the construction of a 2x2 planar antenna array using substrates from [1]. Using recommended available substrates, the antenna element is redesigned and used in the construction of a 2x2 and lastly a 4x4 circularly polarized antenna array optimized for operation in the 24 GHz frequency band.

2. APERTURE COUPLED ANTENNAS

2.1 Conventional aperture coupled antenna

An aperture coupled antenna has two substrates of different material and dielectric constants that are separated by a ground plane with an aperture usually etched at its center. In between the ground plane and the bottom substrate, there is an air gap.

The top substrate is thick with a low dielectric constant whereas the bottom substrate is thin with a high dielectric constant. A radiating element is placed on top of the first dielectric while the feed line is located at the bottom of the second substrate and its energy is coupled to the patch through the slot. This configuration minimizes the interference of spurious radiation for pattern formation and attains polarization purity because of the ground separating the feed and the radiating element [2]. Figure 2.1 below shows the arrangement of an aperture coupled antenna.

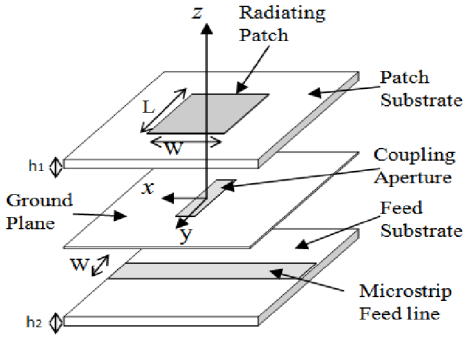

Figure 2.1 Aperture coupled antenna [9]

2.2 Design procedure for an aperture coupled antenna

Assuming the heights and dielectric constants of the substrates and the desired value of the resonant frequency or frequency band of the antenna are known, the following designing procedure is undertaken [2], [5].

1. We calculate the wavelength in the dielectric as follows:

$$\lambda_d = \frac{v_0}{fr\sqrt{0.5(\varepsilon_r+1)}} \tag{2.1}$$

where v_0 is the speed of light in vacuum, ε_r is the permittivity of the dielectric substrate and f_r is the resonance frequency of the antenna.

2. The width of the patch is calculated as:

$$W_p = \frac{\lambda_d}{2} = \frac{v_0}{2fr}\sqrt{\frac{2}{(\varepsilon_r+1)}} \tag{2.2}$$

3. The effective permittivity of the substrate is calculated as

$$\varepsilon_{ef} = \frac{\varepsilon_r+1}{2} + \frac{\varepsilon_r-1}{2}\frac{1}{\sqrt{1+12\frac{h}{W}}} \quad (2.3)$$

where W is the width of the patch and h is the height of the substrate.

4. Due to fringing effects, the patch of the microstrip antenna is electrically longer than its physical dimensions. This means that the length is extended on both sides by a distance ΔL. This extension is calculated as follows:

$$\Delta L = 0.412\frac{(\varepsilon_r+0.3)\left(\frac{W}{h}+0.264\right)}{(\varepsilon_r+0.2580)\left(\frac{W}{h}+0.8\right)}.h \quad (2.3)$$

The actual length of the patch is given by

$$L_p = \frac{v_0}{2f_r\sqrt{\varepsilon_{ef}}} - 2\Delta L \quad (2.4)$$

5. If the patch is fed by a microstrip feed line, we usually design its width in such a way that it will have a characteristic impedance of 50 Ω [5]. To help us in our calculation, we first consider and calculate two parameters a and b as follows:

$$a = \frac{Z_0}{60}\sqrt{\frac{\varepsilon_r+1}{2}} + \frac{\varepsilon_r-1}{\varepsilon_r+1}\left[0.23+\frac{0.11}{\varepsilon_r}\right] \quad (2.6)$$

$$b = \frac{60\,\pi^2}{Z_0\sqrt{\varepsilon_r}} \quad (2.7)$$

where Z_o is the characteristic impedance of the feed line.
We then calculate the width of the feed line as follows:

$$\frac{w}{h} = \frac{8exp(a)}{exp(2a)-2}, \quad a > 1.52 \quad (2.8)$$

$$\frac{w}{h} = \frac{2}{\pi}\left\{b-1-ln(2b-1)+\frac{\varepsilon_{r-1}}{2\varepsilon_r}\left[ln(b-1)+0.39-\frac{0.61}{\varepsilon_r}\right]\right\}, a \leq 1.52 \quad (2.9)$$

6. The nominal value of the length of the aperture is usually taken as half of the wavelength and its width is approximately ten times smaller than the length.

$$L_s = \frac{\lambda_d}{2} \quad (2.5)$$

2.3 Circular polarization in microstrip antennas

The aperture coupled microstrip antenna described so far is primarily linearly polarized and has to be modified to make it circularly polarized. This can be done using certain feeding techniques as shown in Figure 2.2. Circular polarization can be achieved by either using a double or a single feed or by sequential rotation. The aim is to excite two modes that have a phase difference of 90° [2].

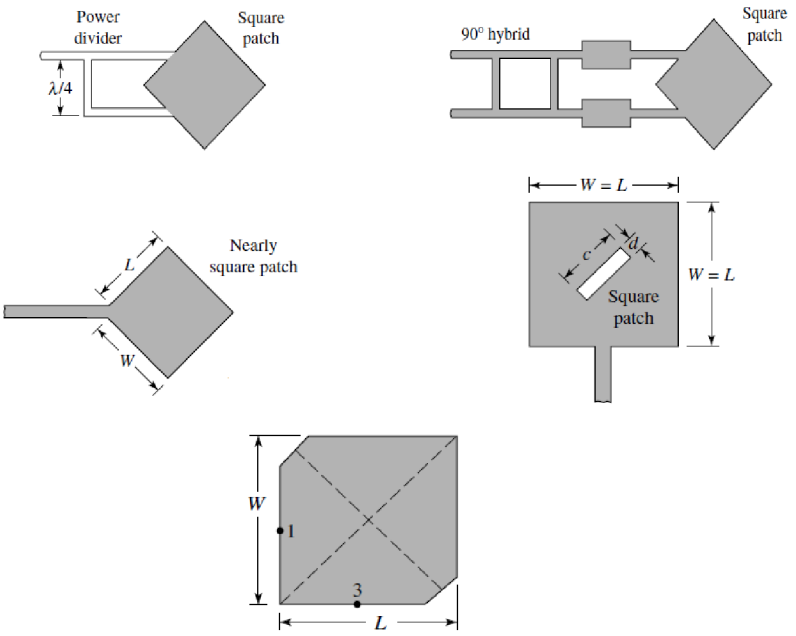

Figure 2.2 Configurations for achieving circular polarization [2]

2.4 Cross-aperture coupled patch antenna

The cross-aperture coupled patch antenna (see Figure 2.3) has three major changes in comparison to the conventional aperture coupled antenna described in section 2.1. Its aperture, coupling the feed and the patch, is in form of a cross to excite two orthogonal modes. The patch, which is separated from the ground plane by an air substrate, is mounted on the bottom layer of the top dielectric. Thirdly, its feed line is with reference to the plane of the patch diagonally positioned. It requires a careful selection of the length and the width of the antenna in order to achieve a phase difference of 90° between the two modes that is necessary for circular polarization [6].

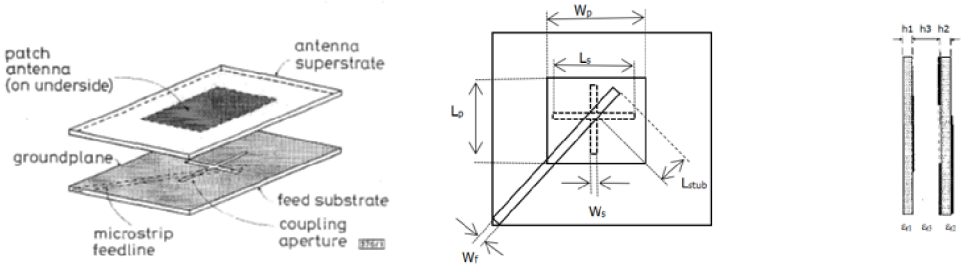

(a) (b) (c)

Figure 2.3 Cross-aperture coupled patch antenna with air substrate [6]
(a) configuration (b) dimensions (c) side view

2.5 Novel circularly polarized antenna element

The novel microstrip antenna element discussed in [1] is shown in Figure 2.4. The element is circularly polarized and designed to operate in the millimeter-wave communication system with reduced polarization mismatch. The element comprises of four metallic patches which are mounted on the top substrate and four metallic posts which ensure that the patches are connected to the ground. Two patches have L-shaped branches and the other two have truncated edges. These adjustments ensure that the conditions necessary for circular polarization to be attained are met [1].

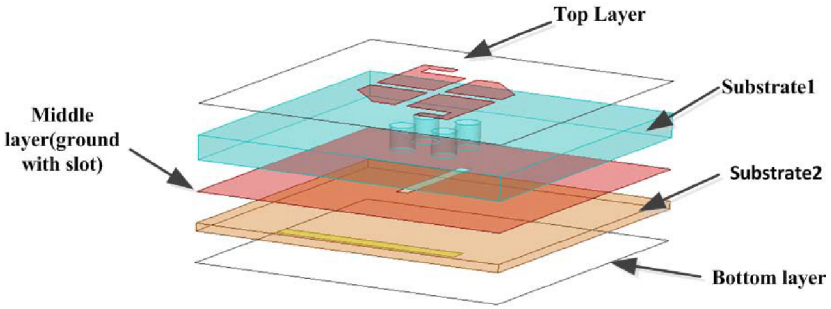

(a)

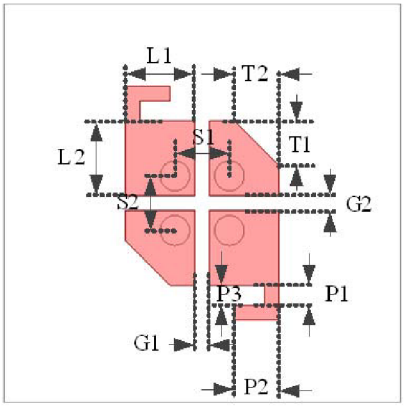

(b)

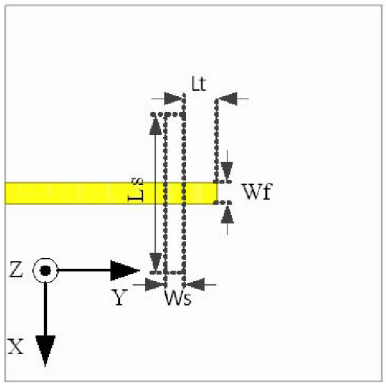

(c)

Figure 2.4 Configuration of the circularly polarized antenna element [1]: (a) Geometrical layers, (b) Top view, (c) Bottom view

3. DESIGN AND SIMULATION OF ANTENNA ELEMENTS

3.1 Design and simulation of the antennas at 45 GHz

Using the design procedure discussed in chapter 2.2, the dimensions of the conventional aperture coupled and the cross-aperture coupled patch antennas were calculated. Their nominal values are shown in Table 3.1(a) below. Table 3.1(b) shows the dimensions of the circularly polarized antenna element from [1]. Using CST Microwave Studio, all three antennas were designed to work at a resonance frequency of 45 GHz. The substrates used are Rogers 5880 (the top substrate) and Rogers 4003(the bottom substrate) with permittivities of 2.20 and 3.55, respectively.

Parameter	Value [mm]
L_p	1.7
W_p	2.6
L_s	2.6
W_s	0.2
h_1	0.8
h_2	0.2
h_3 [1]	0.3
L_{stub}	0.5
L_f	4.0
W_f	0.5
λ_{d1}	5.3
λ_{d2}	4.4

[1] The height h_3 is the height of the air substrate and only applies to the cross-aperture coupled patch antenna. It was calculated using $h \leq \frac{0.3\, v_0}{2\pi f_r \sqrt{\varepsilon_r}}$ [8]

(a)

Parameter	Value [mm]
L_1	1.4
L_2	1.5
S_1	1.1
S_2	1.1
G_1	0.3
G_2	0.3
P_1	0.4
P_2	0.9
P_3	0.3
T_1	0.9
T_2	0.9
L_S	2.6
W_s	0.2
W_f	0.5
λ_{d1}	5.3
λ_{d2}	4.4

(b)

Table 3.1 Nominal values of the antennas:
(a) Conventional aperture coupled antenna and the cross-aperture coupled patch antenna (b) Circularly polarized antenna element

3.1.1 Conventional aperture coupled antenna

Figure 3.3, 3.2 and 3.3 show the results of the simulation of the conventional aperture coupled antenna for the nominal values. The resonance frequency was 43.825 GHz, the impedance bandwidth was 5% for a return loss lower than -10 dB (frequencies from 42.625 GHz to 45.025 GHz) and maximum gain and directivity of 8.55 dB and 7.09 dB, respectively.

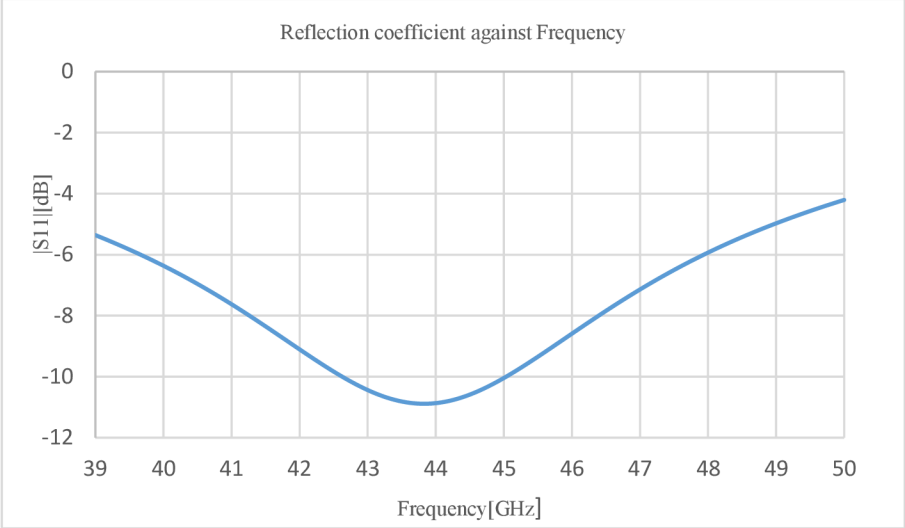

Figure 3.1 Frequency characteristics of reflection coefficient for nominal values of conventional aperture coupled antenna

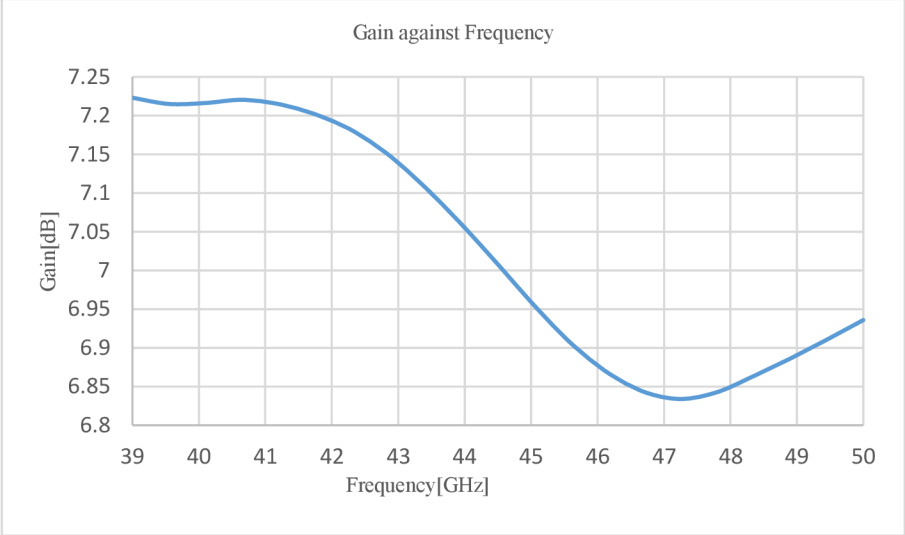

Figure 3.2 Frequency characteristics of gain for nominal values of conventional aperture coupled antenna

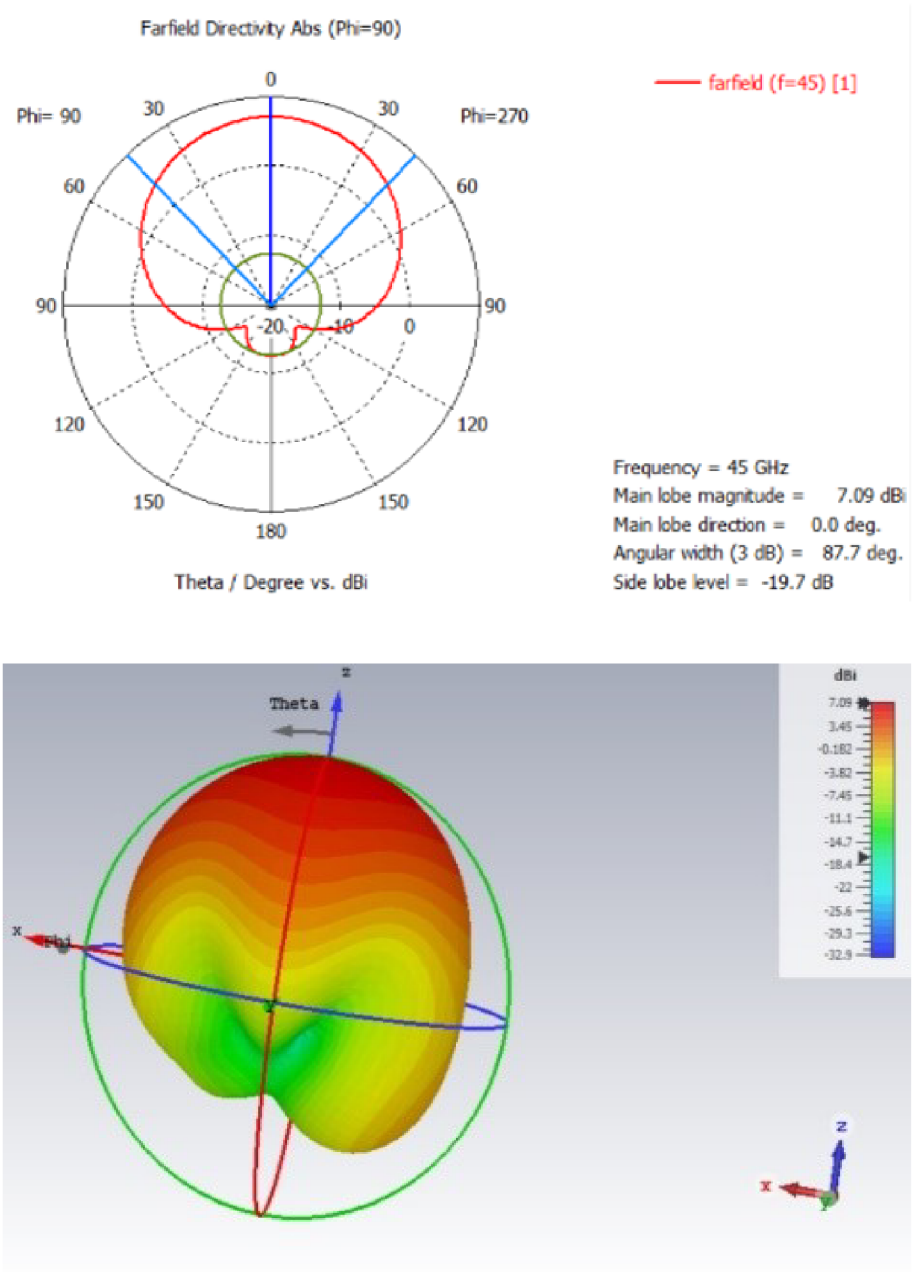

Figure 3.3 Farfield directivity at 45 GHz. Top: polar coordinates, Bottom: 3-dimensional characteristics

A parametric analysis was done to find out the effect of the parameters on the overall performance of the antenna. Figure 3.4 and Figure 3.5 show the results of the parametric analysis and the final optimized results, respectively.

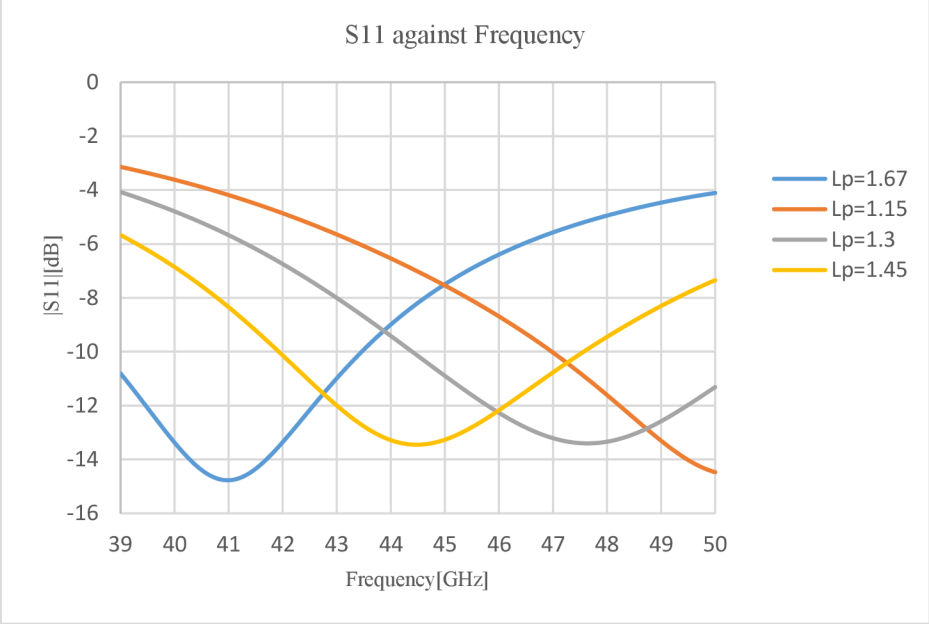
S11 against Frequency
0
-2
-4
-6
-8
-10
-12
-14
-16
|S11|[dB]
39 40 41 42 43 44 45 46 47 48 49 50
Frequency[GHz]
Lp=1.67
Lp=1.15
Lp=1.3
Lp=1.45

(a)

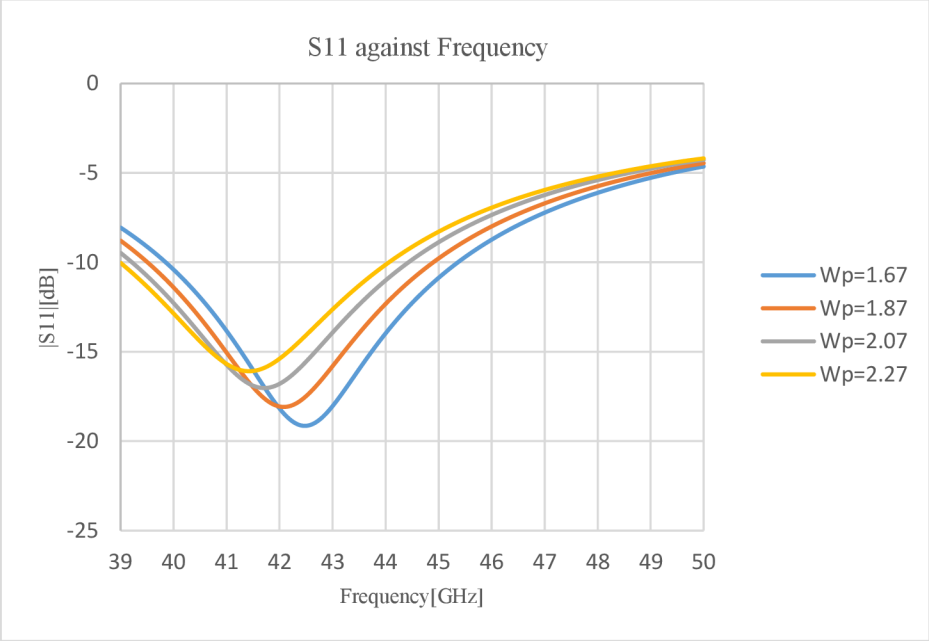
S11 against Frequency
0
-5
-10
-15
-20
-25
|S11|[dB]
39 40 41 42 43 44 45 46 47 48 49 50
Frequency[GHz]
Wp=1.67
Wp=1.87
Wp=2.07
Wp=2.27

(b)

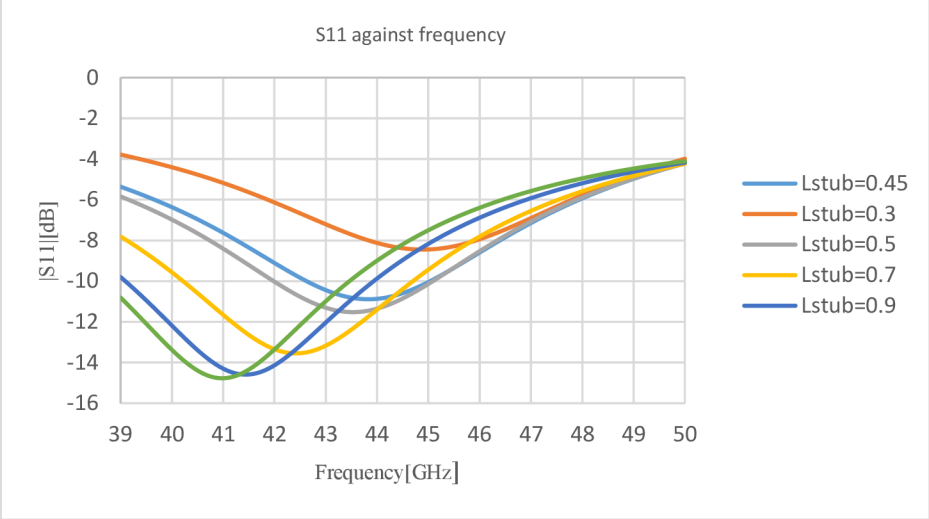

(c)

Figure 3.4 Parametric analysis of length of the patch(a), width of the patch , length of the stub of the microstrip line(c)

The results of the analysis show that increasing the length of the stub improves impedance matching, increases the bandwidth, and reduces the resonance frequency. Reducing the length of the patch increases resonance frequency and the increase of its width increases bandwidth with the effect of moving the frequency upwards. Putting these into consideration, the resonance frequency was finally tuned to 45.03 GHz. Figure 3.5 shows the frequency characteristic of S11 and gain and the radiation pattern of the optimized antenna while Table 3.2 summarizes its optimal parameters.

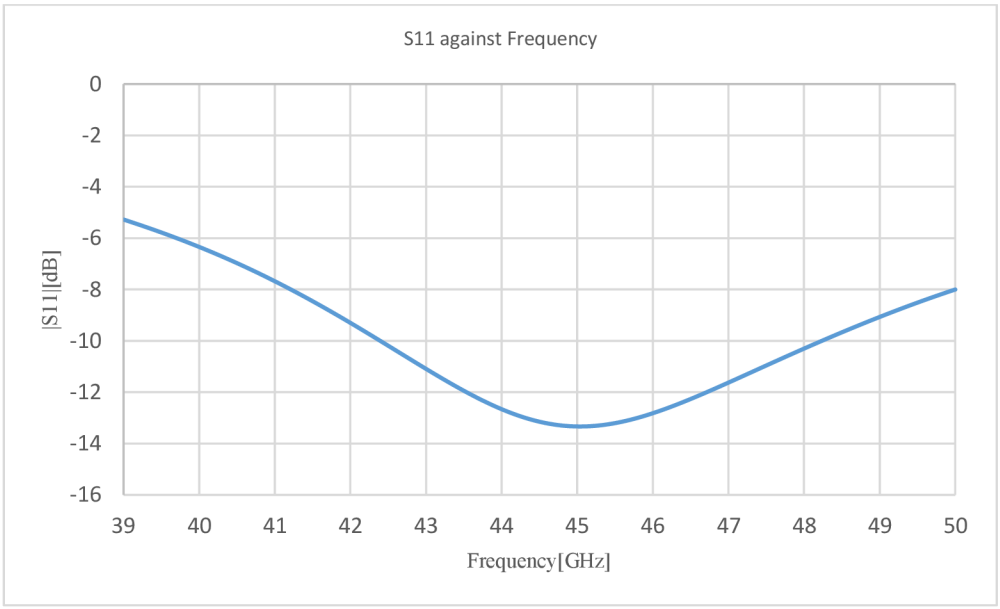

(a)

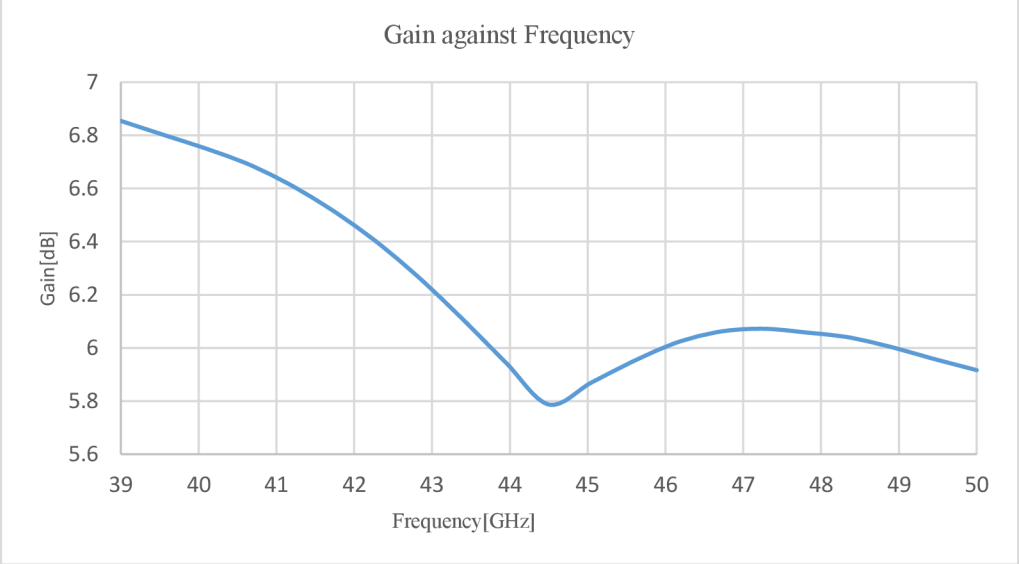

(b)

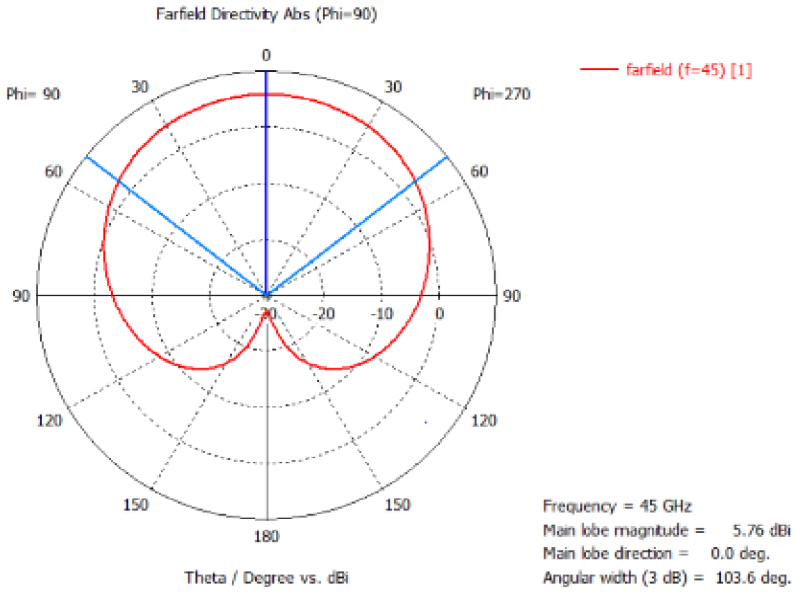

(c)

Figure 3.5 Final performance of the antenna: (a) S11 (b) Gain (c) Far-field directivity at 45 GHz

The results of the simulation are in conformity with the theoretical assumption of performance. This antenna is linearly polarized and its simulation therefore served as a verification of the functionality of a conventional aperture coupled antenna and as a basis for designing circularly polarized antennas. The following sections will focus on the simulation of the circularly polarized antennas.

Parameter	Value [mm]
L_p	1.4
W_p	2.6
L_s	2.6
W_s	0.2
h_1	0.8
h_2	0.2
L_{stub}	1.0
L_f	4.0
W_f	0.5

(a)

Parameter	Value
Bandwidth	12.96 %
Maximum Gain	8.05 dB
Directivity	5.76 dBi

(b)

Table 3.2 (a) Final antenna dimensions, (b) performance parameters

3.1.2 Cross-aperture coupled patch antenna

The results of the simulation of the antenna at its nominal parameters were not good. The antenna impedance was not matched, and its circular polarization was not acceptable. To improve its performance, parameters of the antenna were adjusted. The air substrate had an effect of reducing backward radiation but increasing the height of the air gap reduced the impedance matching. The height of the air substrate was adjusted to around $\frac{1}{20}\lambda_{d2}$ after a parametric analysis.

Increasing the length of the aperture while reducing its width tended to improve coupling and impedance matching while reducing circular polarization of the antenna, and vice versa. Increasing the length of the stub had a similar effect.

Figure 3.6 and Figure 3.7 show the final optimized results of the antenna performance.

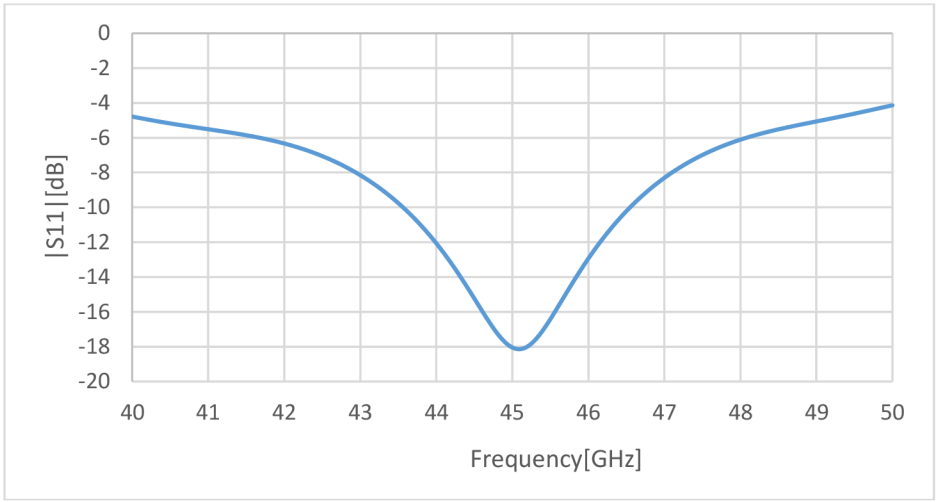

(a)

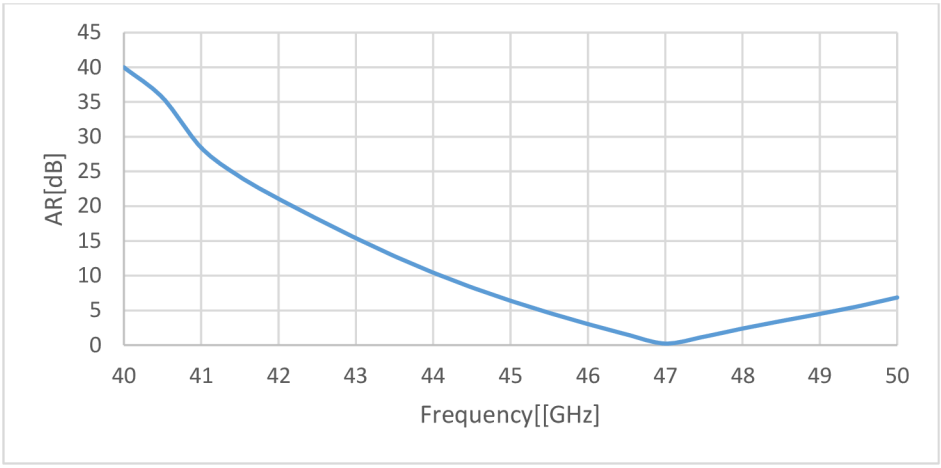

(b)

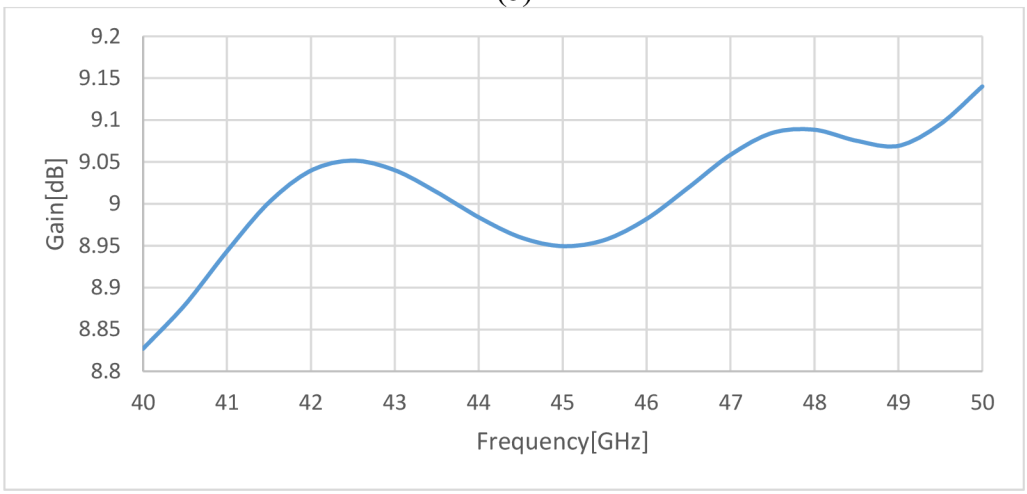

(c)

Figure 3.6 Cross-aperture coupled patch antenna performance: (a) Reflection coefficient, (b) Axial ratio, (c) Gain

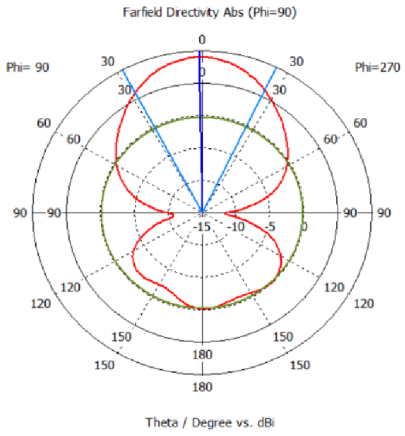

(a)

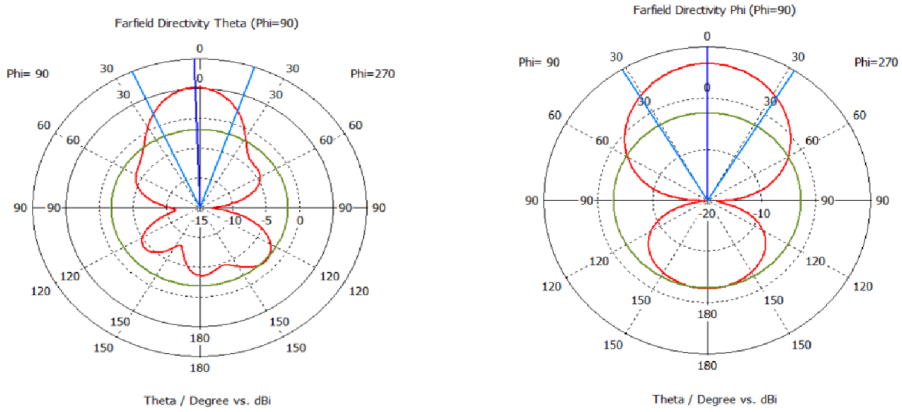

(b) (c)

Figure 3.7 Radiation pattern of cross-aperture coupled antenna at 45 GHz: (a) absolute value, (b) Theta component, (c) Phi component

Resonance frequency of 45.09 GHz was achieved. The antenna had an impedance bandwidth of 6.4% for a frequency range from 43.6 GHz to 46.6 GHz and a 3 dB AR bandwidth of 5.3% for frequencies from 46 GHz to 48. 4 GHz. The 45 GHz frequency was not covered in the 3dB AR bandwidth but lies in the 6dB AR bandwidth. This antenna also shows quite strong backward radiation. Table 3.1(b) summarises its performance.

Parameter	Value [mm]
L_p	2.0
W_p	2.6
L_s	4.5
W_s	0.03
h_1	0.8
h_2	0.2
h_3	0.3
L_{stub}	1.3
L_f	5.0
W_f	0.5
W	7.5
L	7.5
λ_{d1}	5.3
λ_{d2}	4.4

(a)

Parameter	Value
Bandwidth	6.4%
AR Bandwidth	5.3%
Maximum Gain	9.01dB
Directivity	8.02 dBi

(b)

Table 3.3 Final parameters of the cross-aperture coupled patch antenna: (a) Dimensions, (b) Performance parameters

3.1.3 Novel circularly polarized antenna element

The magnitude of the radius of the metallic posts was not given in [1]. It was observed that it has an impact on the overall radiation performance of the antenna, particularly on reflection coefficient, bandwidth and resonance frequency as shown in Figure 3.8. The impedance matching of the antenna improves as the radius of posts reduces within the range of 0.40 mm to 0.30 mm. On the contrary, the bandwidth and resonance frequency are reduced. Above the radius value 0.44 mm, reflection coefficient was above -10 dB for the whole examined frequency band from 39 GHz to 55 GHz. The radius of 0.3 mm was used in final simulated results.

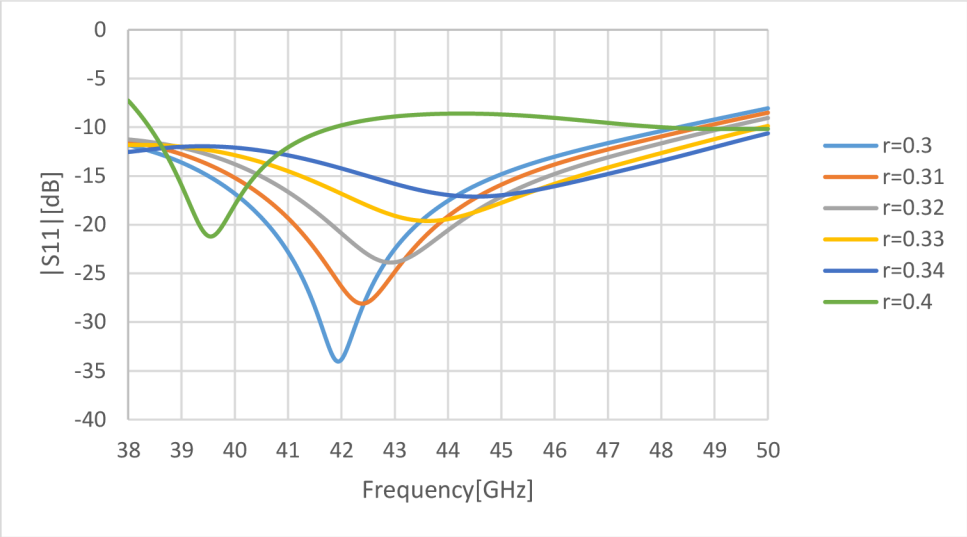

Figure 3.8 The effect of the radius of the metallic posts on reflection coefficient at the input of novel circularly polarized antenna

The final results of the simulation of the reflection coefficient were in agreement with the results published in [1] .The simulated impedance bandwidth was 25.1% while that from [1] was 24.9%. The axial ratio however showed a difference .The simulated 3 dB AR bandwidth was 14.3% while that from [1] was 17.3%.

Figure 3.9 and Figure 3.10 show the simulated results and the published results respectively. The antenna shows wide bandwidths with good circular polarization and also shows good radiation pattern with small backward radiation.

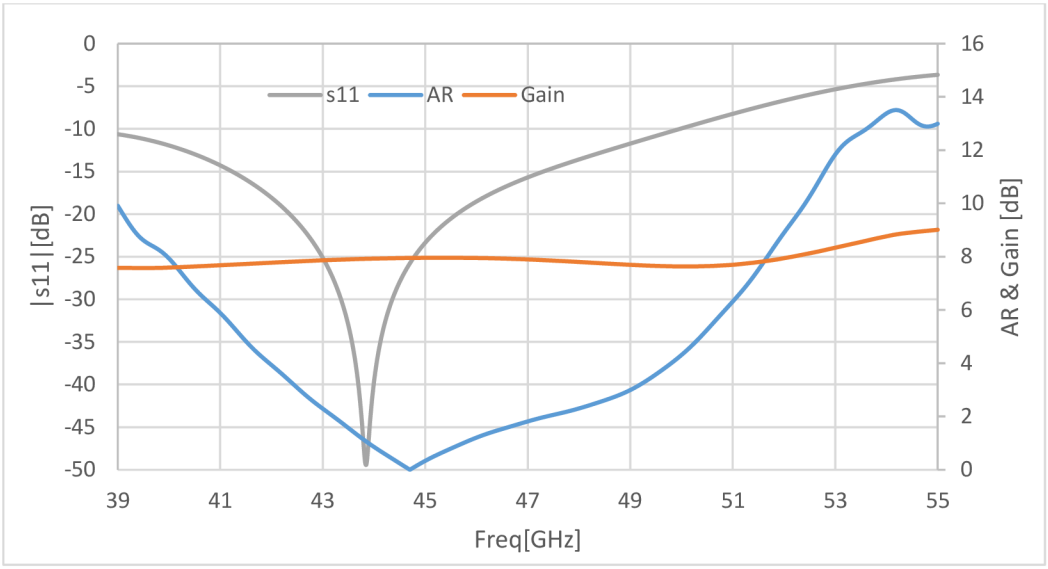

Figure 3.9 Simulated frequency response of reflection coefficient (grey), axial ratio (blue) and gain (orange) of novel circularly polarized antenna

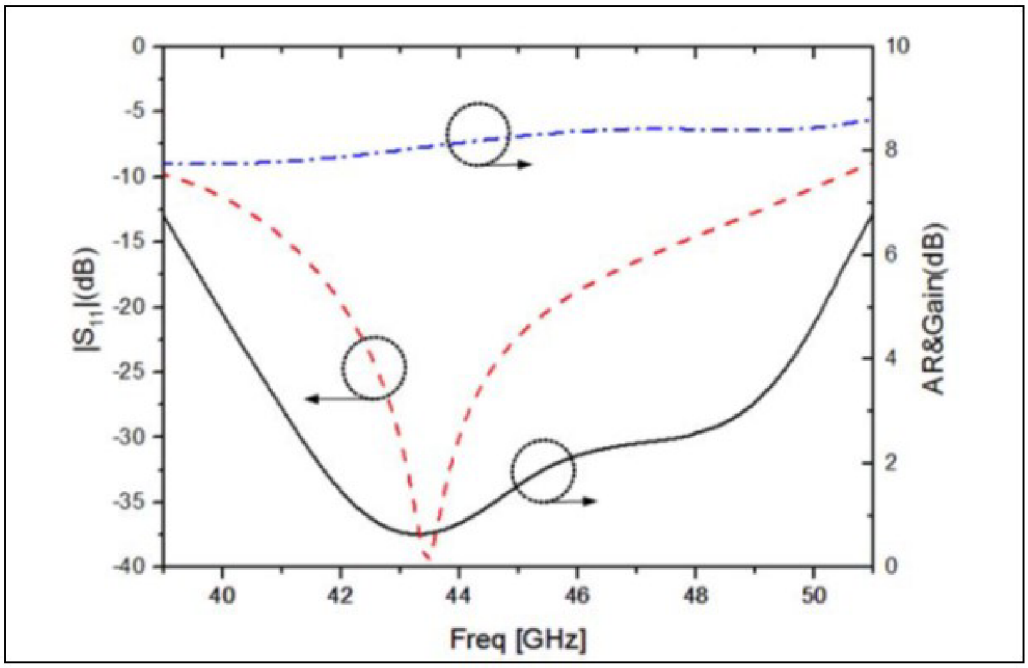

Figure 3.10 Frequency response of reflection coefficient (orange), axial ratio (black) and gain (blue) of the novel antenna from [1]

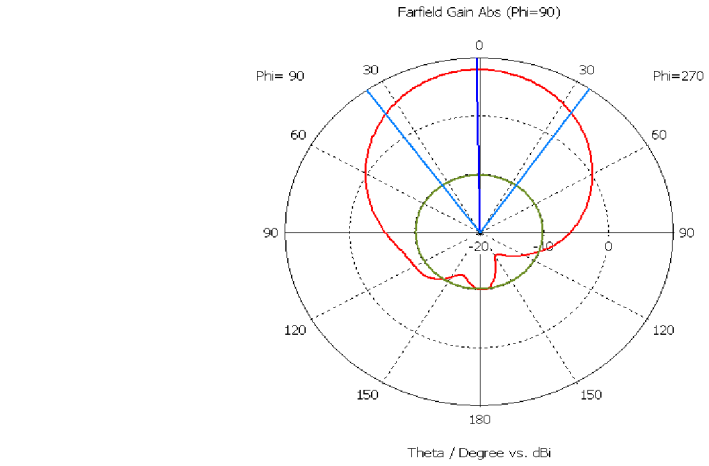

(a)

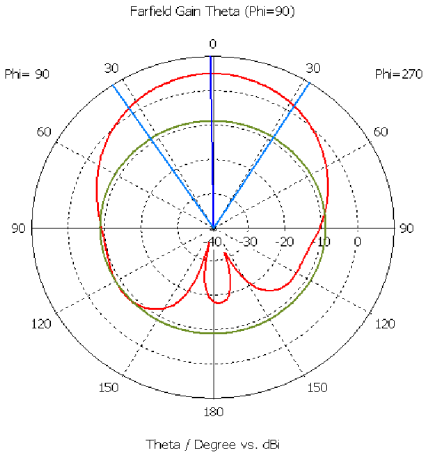

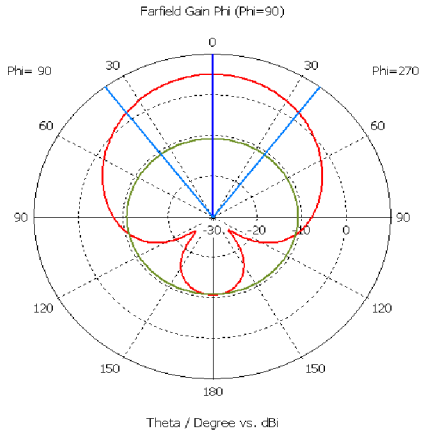

(b) (c)

Figure 3.11 Simulated radiation pattern of the novel antenna at 45 GHz: (a) absolute value, (b) Theta component, (c) Phi component

3.1.4 Comparison of performance between the circularly polarized antennas

The results show that the novel CP antenna element has better performance compared to the cross-aperture coupled patch antenna. The novel element has an impedance bandwidth of 25.1 % (over a frequency range from 39 GHz to 50 GHz) that is wider compared to the 6.4% impedance bandwidth of the cross-aperture coupled patch antenna.

The new element also shows a better radiation efficiency and a lower backward radiation. However, its peak gain is lower.

Table 3.4 shows a full comparison of all the simulated antennas. Owing to its better performance, the novel CP microstrip antenna element is more suitable for use in the design of an antenna array operating in the 24 GHz ISM frequency band.

Parameter	Cross-aperture coupled antenna	Novel CP element
	Value	Value
Impedance bandwidth (|S11|<-10dB)	6.4%	25.1%
AR bandwidth (3dB)	5.3%	14.3%
Peak Gain	9.01 dB	8.0 dB
Directivity	9.04 dB	8.02 dB
Minor lobe level	-9.2 dB	-18.0 dB

Table 3.4 Comparison of performance of the circularly polarized antennas

3.2 Design and simulation of the novel CP element at 24 GHz

Since the antenna array is supposed to operate in the 24 GHz frequency band, the parameters of the CP microstrip antenna element are recalculated so that it can resonate at that frequency. Firstly, its length and width are increased by a factor of 2, the dimensions of the feed line are recalculated using equations 2.6 to 2.9 and the slot length is recalculated using equation 2.10. The remaining parameters are similar to the those of the antenna operating at 45 GHz. A parametric analysis is then done to find out the effect of the truncated corners (*T1* and *T2*), the spacing on the patch (*G1* and *G2*) and the L-shaped branches (*P1* and *P2*). Only one parameter at a time is changed while keeping the rest constant.

3.2.1 Truncated corners (*T1, T2*)

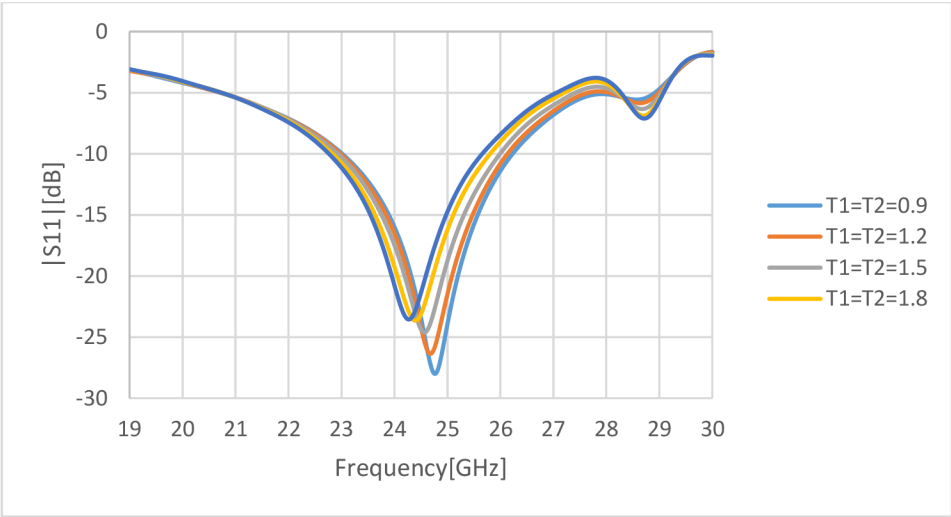

(a)

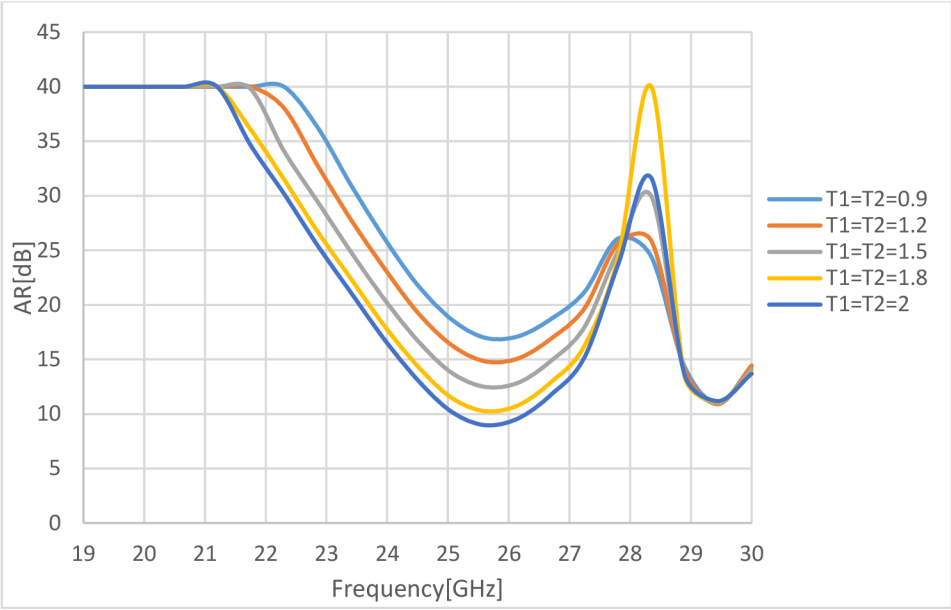

(b)

Figure 3.12 Effect of truncated corners on parameters of the novel element: (a) reflection coefficient, (b) axial ratio

Increasing the amount of truncation, i.e. increasing *T1* and *T2*, the axial ratio is reduced, and vice versa (see Figure 3.12). The amount of improvement on the axial ratio was however limited by geometrical factors, i.e. *T1* and *T2* could not be increased such that they would be greater than the length and the width of the patch. Increasing the level of truncation also slightly reduced the resonance frequency and slightly increased the reflection coefficient.

3.2.2 Space between the patches (*G1, G2*) and the distance between metallic posts (*S1, S2*)

To find out the effect of the space between the patches, the effect of the position of the four metallic posts had to be determined first because increasing the amount of space requires the metallic posts to be moved as well. Increasing the distance between the posts showed an improvement in the axial ratio but at the expense of the reflection coefficient as it greatly increased (Figure 3.13). At a value of $S1 = S2 = 1.5$ mm, S11 was already above -10 dB for the whole examined frequency band (from 19 GHz to 30 GHz). This shows that it is good to have a small distance between the posts.

Setting a reasonable distance between the posts, the effect of the space between the patches could be examined in the range of 0.04 mm $< G1 = G2 <$0.3 mm. Increasing the space increased the impedance bandwidth, the resonance frequency and the axial ratio, and vice versa. Out of this range, the axial was very high and the reflection coefficient was above -10 dB.

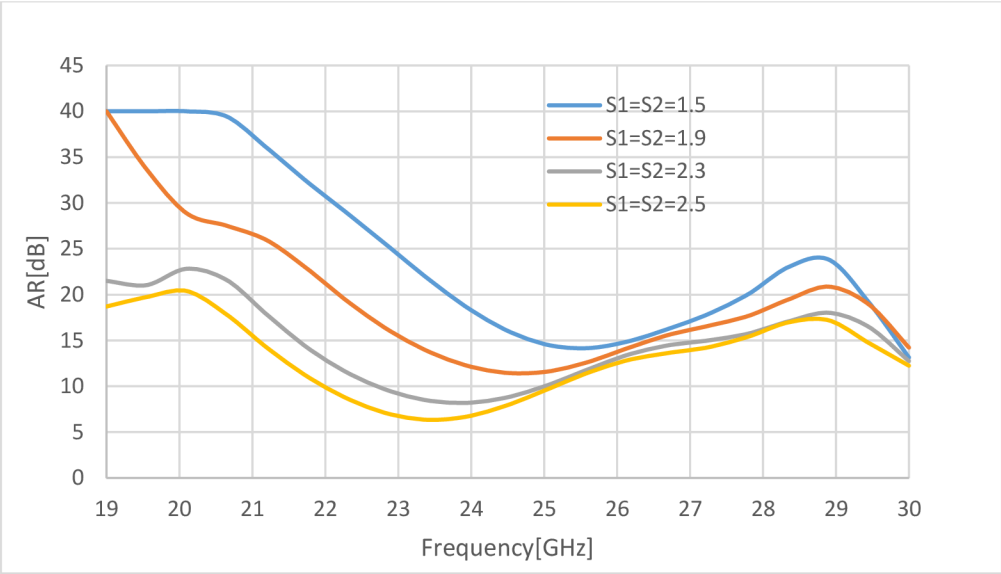

(a)

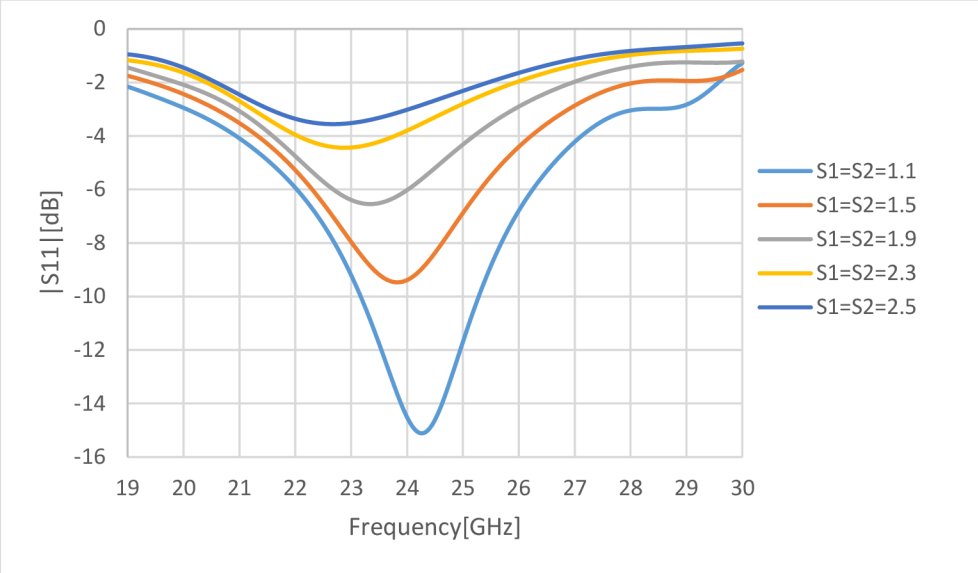

(b)

Figure 3.13 Effect of *S1* and *S2* on parameters of the novel element: (a) axial ratio, (b) reflection coefficient

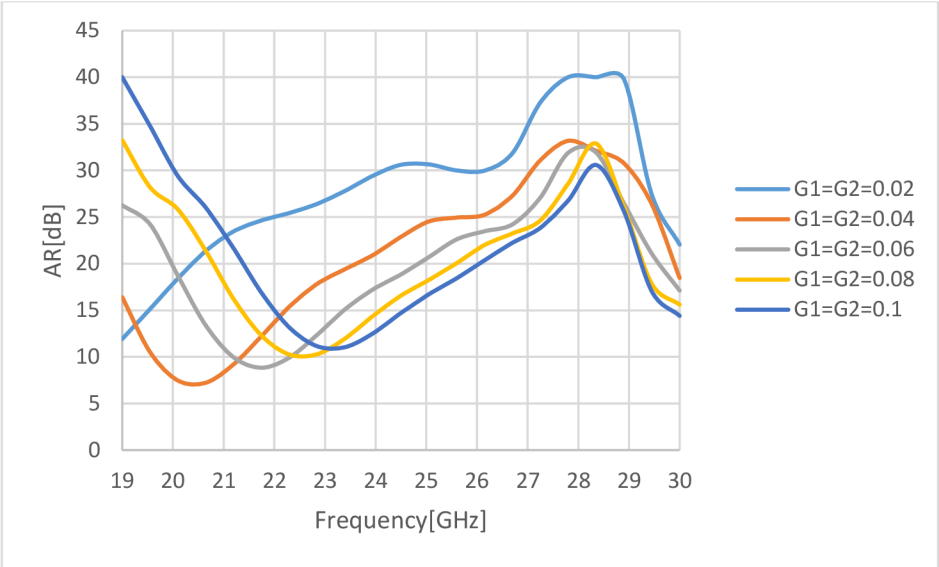

(a)

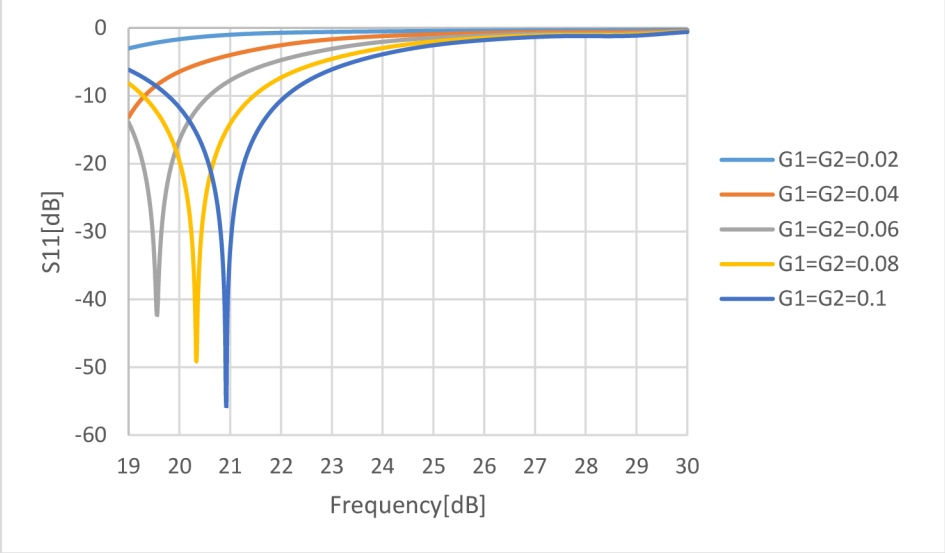

(b)

Figure 3.14 Effect of *G1* and *G2* on parameters of the novel element: (a) axial ratio, (b) reflection coefficient

3.2.3 L-shaped branches (*P1*, *P2*)

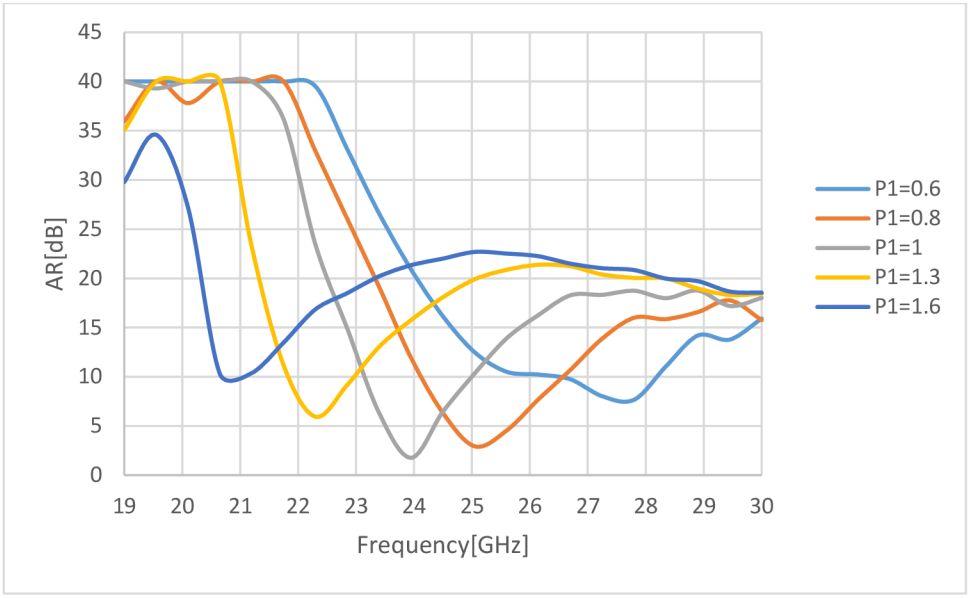

(a)

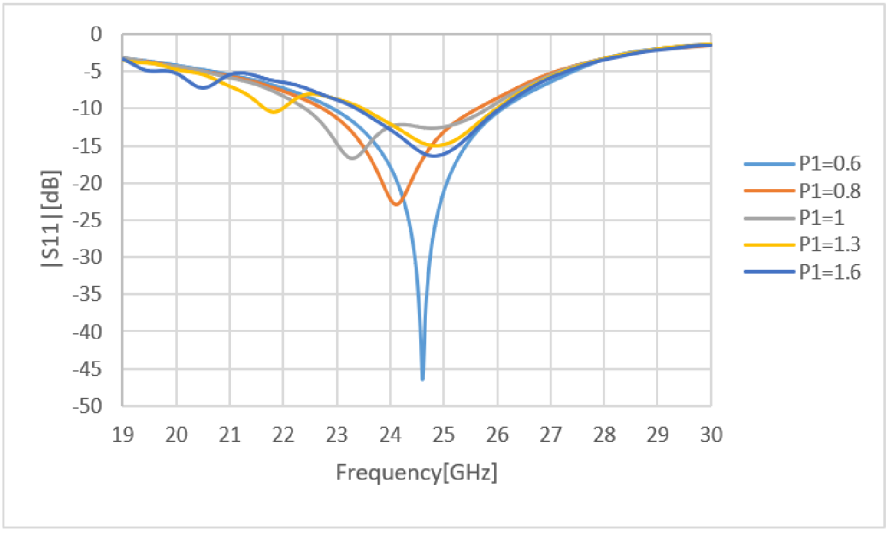

(b)

Figure 3.15 Effect of *P1* on parameters of the novel element: (a) axial ratio, (b) reflection coefficient

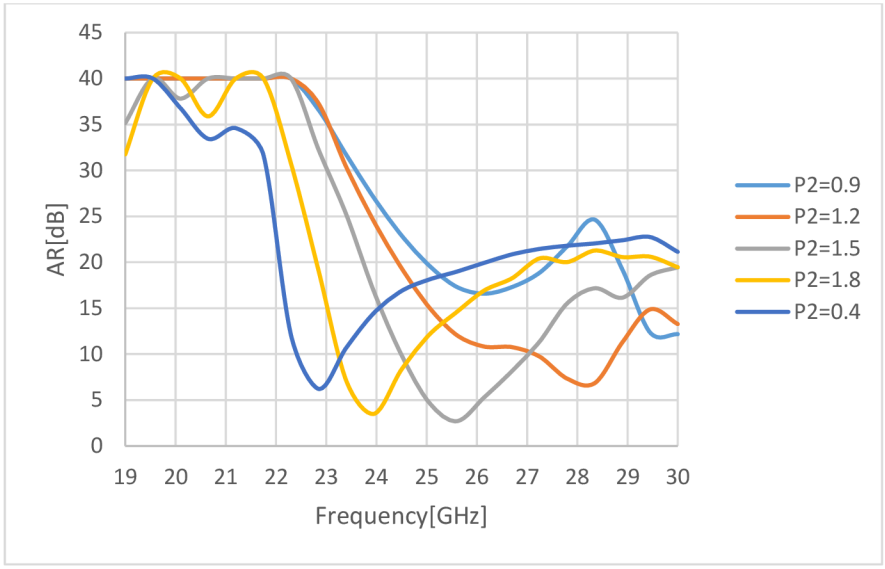

(a)

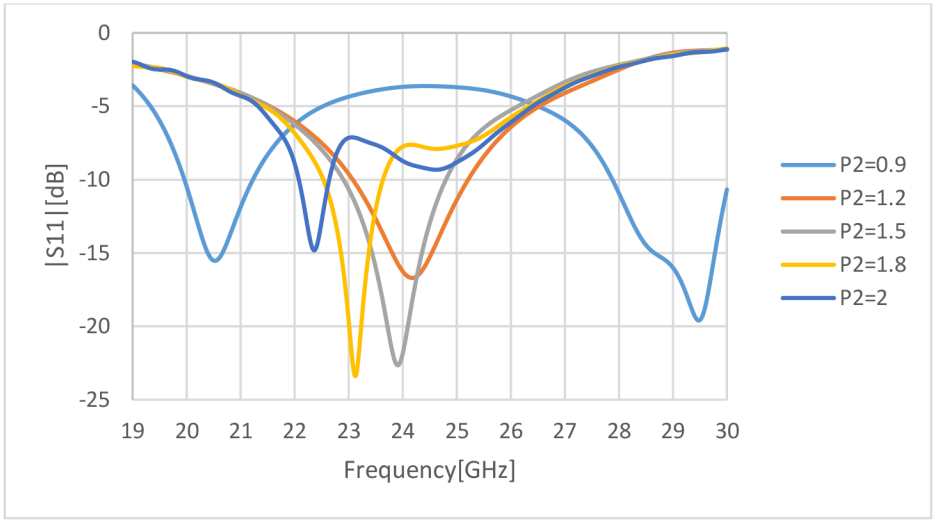

(b)

Figure 3.16 Effect of *P2* on parameters of the novel element: (a) axial ratio, (b) reflection coefficient

The effect of the L-shaped branches can be seen from Figure 3.15 and Figure 3.16 .Increasing the length of *P1* in the range of 0.6 mm to 1.6 mm reduces the resonance frequency and improves the axial ratio. Although the magnitude of the reflection coefficient reduces (i.e. improves at the resonance frequency), the impedance bandwidth remains relatively the same.

The length of *P2* was examined in the range 0.4 mm to 1.8 mm. Just like the length *P1*, *P2* reduces the resonance frequency, improves the axial ratio, and has a very small effect on the impedance bandwidth as its length increases. Out of this range, it caused the antenna to resonate at two different frequencies in the frequency band 19 GHz to 30 GHz.

The lengths *P1* and *P2* can therefore be used to tune the antenna but only in a limited range of values.

3.2.4 Optimal results

The novel antenna element was optimized, and the following results were obtained as shown in Figure 3.17 to Figure 3.19.

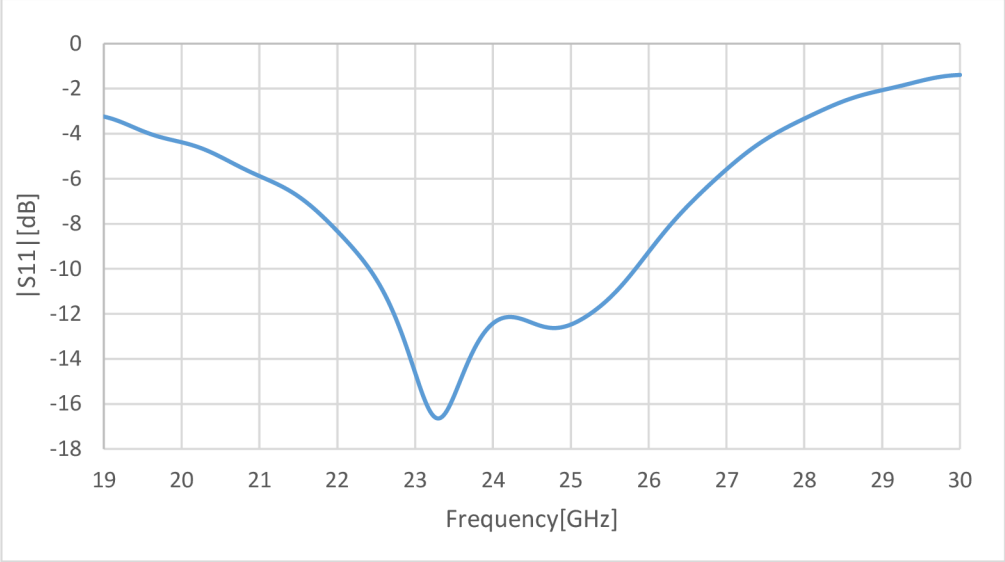

Figure 3.17 Frequency response of reflection coefficient of the novel optimized antenna element

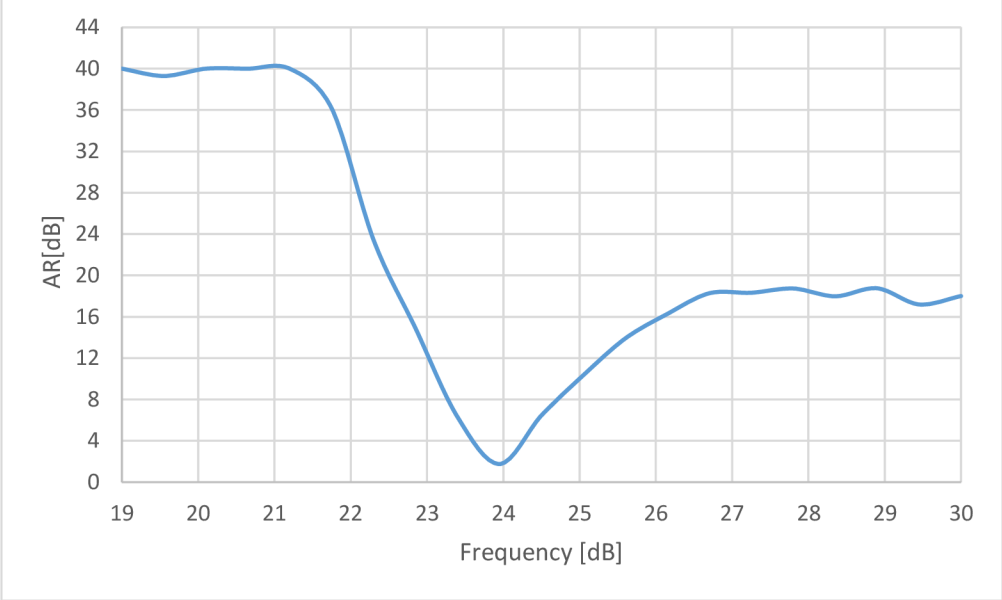

Figure 3.18 Frequency response of axial ratio of the novel optimized antenna element

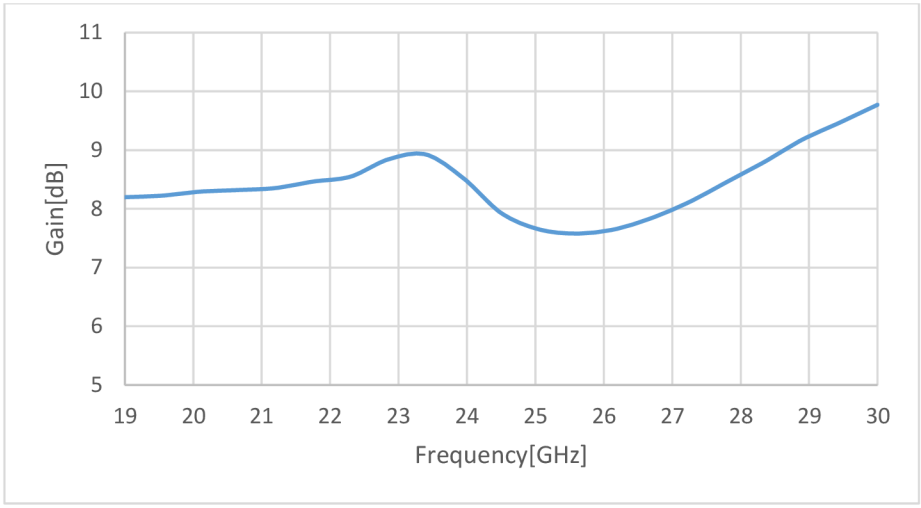

Figure 3.19 Frequency response of gain of the novel optimized antenna element

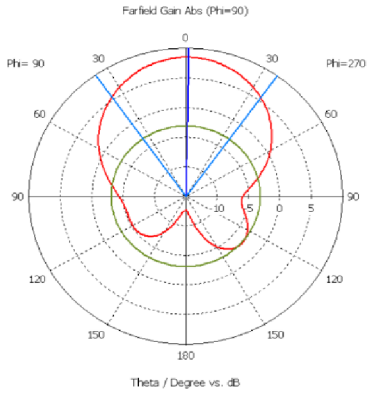

(a)

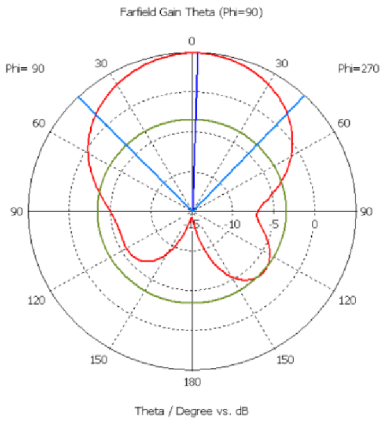

(b)

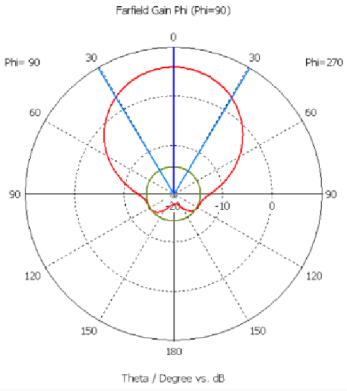

(c)

Figure 3.20 Radiation pattern of the novel optimized antenna element at 24 GHz: (a) Absolute gain (b) Theta component (c) Phi component

The antenna has the impedance bandwidth 14.3% for a frequency range from 22.4 GHz to 25.8 GHz and the 3 dB AR bandwidth 1.4% for a frequency range from 23.8 GHz to 24.14 GHz. The gain is above 7.4 dB for the frequency range from 19 GHz to 30 GHz. The antenna also shows low backward radiation.

Parameter	Value [mm]
L_1	3.0
L_2	3.2
S_1	1.1
S_2	1.1
G_1	0.3
G_2	0.3
P_1	1.0
P_2	0.9
P_3	0.3
T_1	0.9
T_2	0.9
Ls	3.4
Ws	0.2
W_f	0.5
L_t	1.3
L_f	9.0
r	0.3

(a)

Parameter	Value
Bandwidth(|s11|<10dB)	14.2%
3dB AR Bandwidth	1.4%
Maximum Gain	8.8dB

(b)

Table 3.5 The novel optimized antenna element: (a) Dimensions, (b) Performance parameters

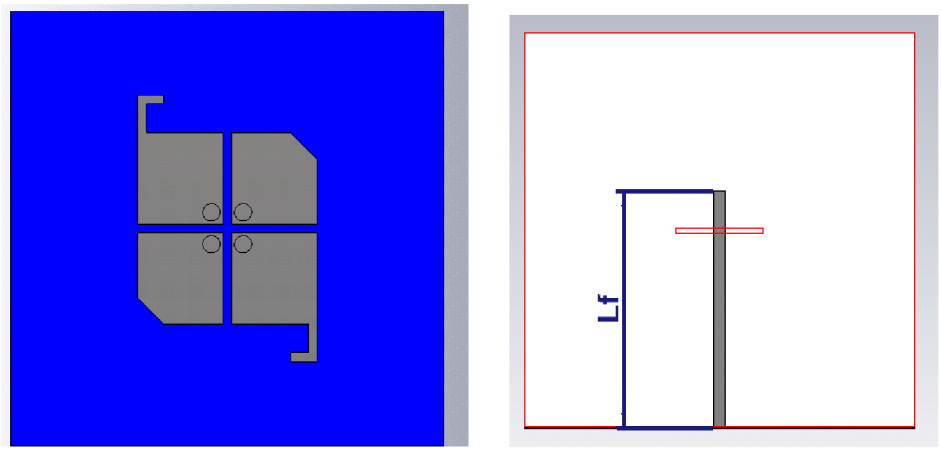

(a) (b)

Figure 3.21 Numerical model of the simulated antenna element in CST Microwave Studio: (a) Top view, (b) bottom view

4. NOVEL 2×2 CP ANTENNA ARRAY AT 24 GHz

4.1 Original substrates

The 2x2 antenna array was initially designed with the elements separated by the distances equal to the size of the wavelength in the top substrate. Its design in CST Microwave Studio is shown in Figure 4.1.

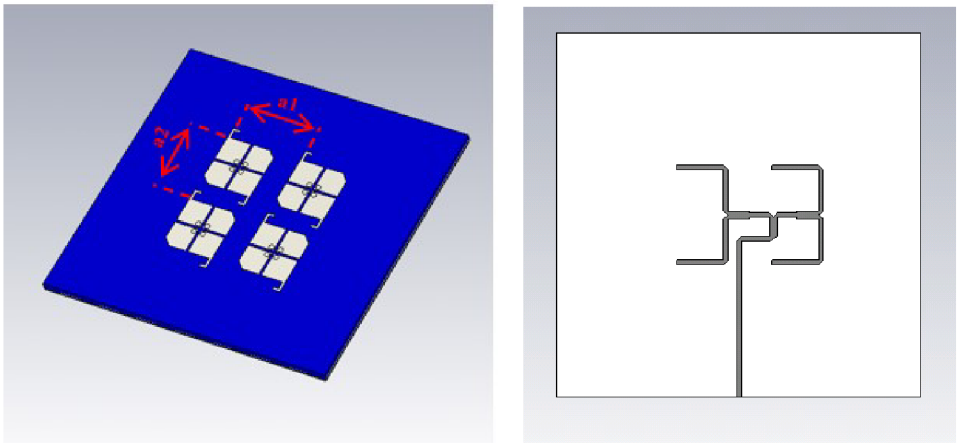

Figure 4.1 Numerical model of the 2×2 antenna array in CST Microwave Studio: (a) top view, (b) bottom view

The simulation of the antenna array on original substrates from [1] was done in CST Microwave studio 2018 using the time domain solver with a hexahedral mesh, steady state accuracy limit -40 dB and used time step width 1.535e^{-4} ns. The rest of the mesh property settings are shown in the figure below. The settings were done with the aim of maintaining a balance between accuracy and speed of the simulation [10], [11].

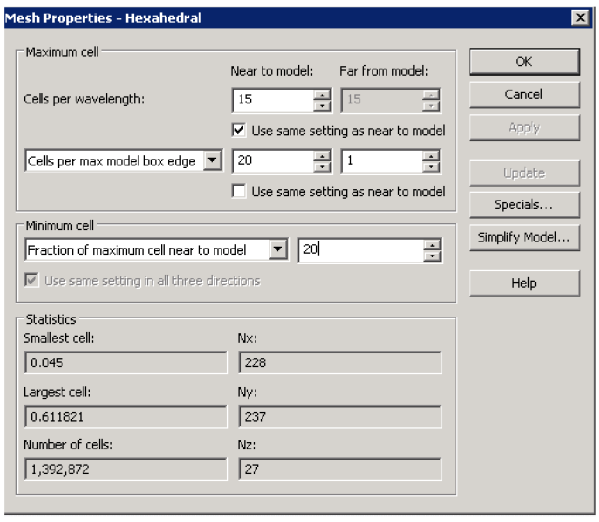

Figure 4.2 Mesh properties for the 2×2 antenna array on original substrates

It was observed during simulations that the parameters *a1* (inter-element spacing in the x-axis) and *a2* (inter-element spacing in the y-axis) affect the axial ratio, reflection coefficient and gain of the antenna array. The parameter *Lt* was mainly used for impedance matching (improving the impedance bandwidth). Reducing the length *a1* while keeping *a2* constant and vice versa, improved the radiation pattern by reducing the side lobe level but reduced the axial ratio bandwidth and gain of the antenna.

An optimization sweep (Trust Region Framework algorithm) was therefore done for parameters *a1*, *a2* and *Lt*. After optimization, the distances *a1* (in the x-axis) and *a2* (in the y-axis) between the elements are set to 9.1 mm.

The optimal results of the simulation of frequency characteristics of the reflection coefficient, axial ratio and gain of the antenna array are shown in Figure 4.3 to Figure 4.5.

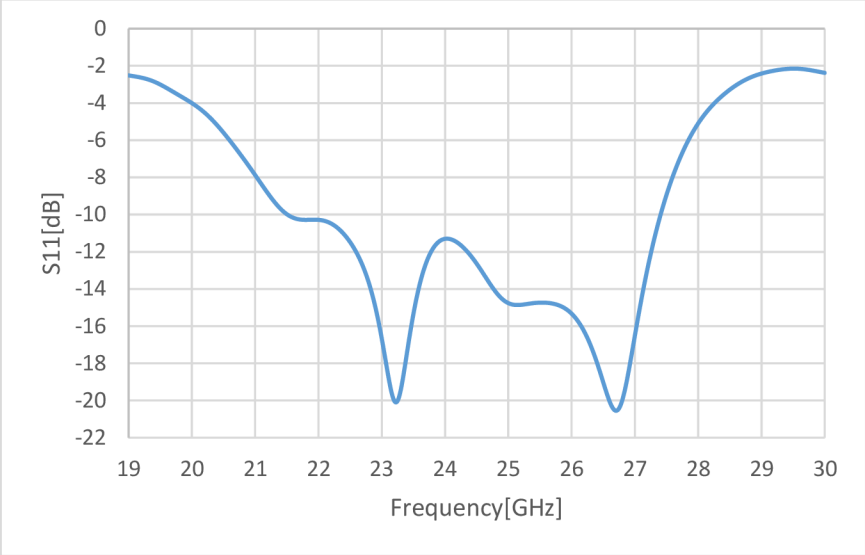

Figure 4.3 Reflection coefficient of the 2×2 antenna array on original substrates

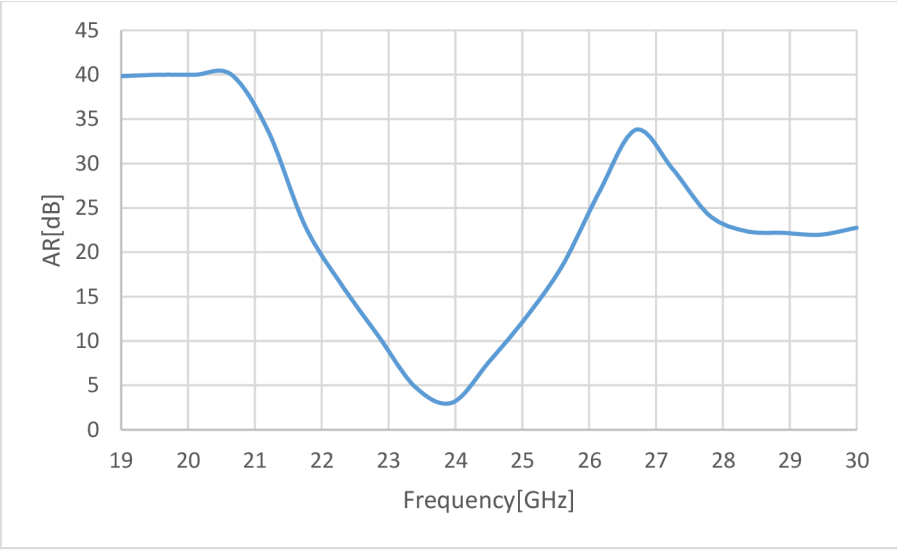

Figure 4.4 Axial ratio of the 2×2 antenna array on original substrates

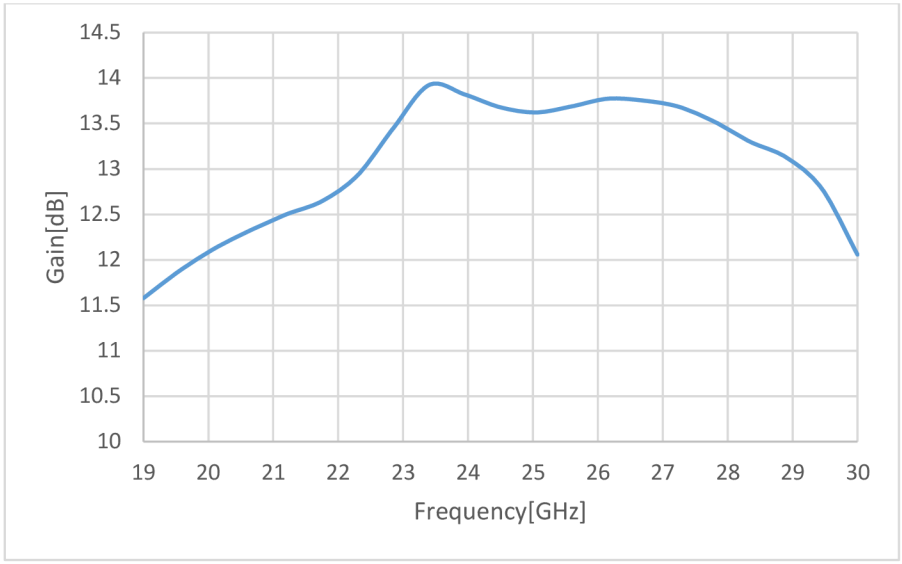

Figure 4.5 Gain of the2×2 antenna array on original substrate

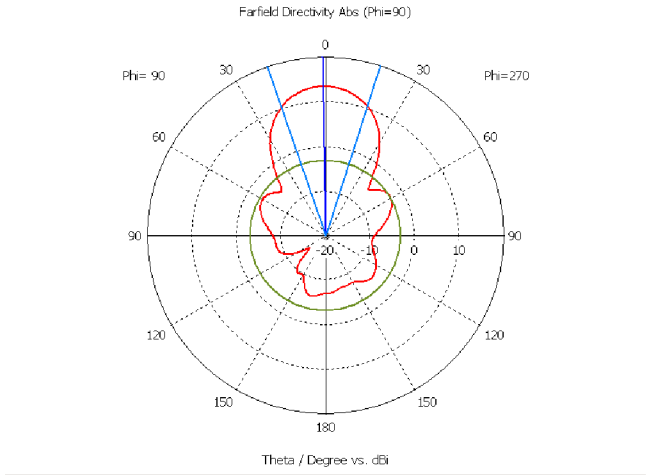

(a)

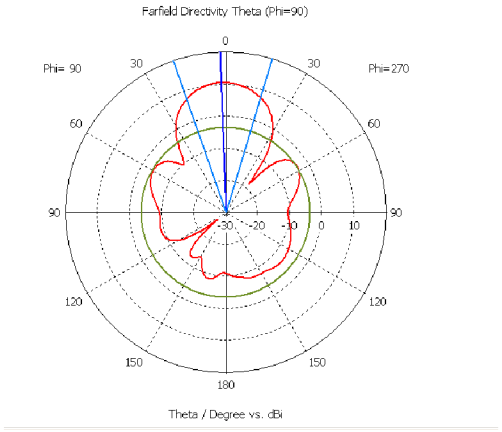

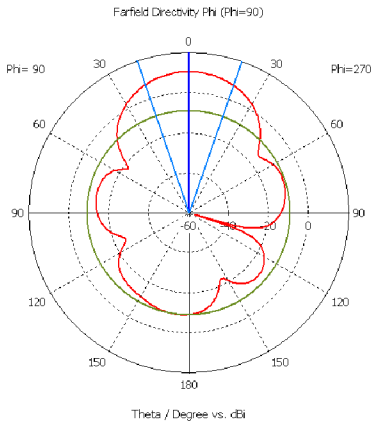

(a) **(b)**

Figure 4.6 Radiation pattern of the 2×2 antenna array on new substrates: (a) Absolute radiation, (b) Theta component, (c) Phi component

Parameter	Value
Bandwidth (|S11|<-10 dB)	24.6 %
6 dB AR Bandwidth	3.84 %
Maximum Gain	13.9 dB

Table 4.1 Results of simulation of the 2×2 antenna array on original substrates

Parameter	Value [mm]
L_1	3.0
L_2	3.2
S_1	1.1
S_2	1.1
G_1	0.3
G_2	0.3
P_1	1.0
P_2	0.9
P_3	0.3
T_1	0.9
T_2	0.9
L_S	3.4
W_s	0.2
W_f	0.5
S	2.7
L	35
W	35
L_t	1.5

Table 4.2 Dimensions of the optimized 2x2 antenna array on original substrates

The results of the antenna array show a wide impedance bandwidth (24.6%) and relatively high gain (13.9 dB). Although the axial ratio of 3.0 dB was achieved at the operating frequency, the rest of the examined frequency range had an axial ratio higher than 3 dB. The 6 dB axial ratio bandwidth was therefore considered. Its value was 3.84 % as shown in Table 4.1. By reducing the separation distance between the elements, the results can be improved. However, the inter-element distance cannot be reduced because of the limited attainable compactness of the microstrip feeding network.

The performed simulation verified the functionality of the antenna array proposed in [1]. The antenna was then redesigned using available recommended substrates (see chapter 4.2).

4.2 Available substrates

As was alluded to in the preceding sub-chapter, the antenna was redesigned using recommended available substrates. The substrate Cuclad217 (ε_r = 2.17, tan δ = 0.0009) was used for both the top layer and the bottom layer with heights h_1 = 1.54 mm and h_2 = 0.254 mm, respectively. By using a thinner height for the bottom substrate, the width of the feed was minimized, implementing a more compact feed network for the antenna array.

Similar to the preceding sub-chapter, the transient solver with a hexahedral mesh, steady state accuracy limit -40 dB, and used time step width 1.279e^{-4} ns is used for the simulation of the 2x2 antenna array on available substrates in CST Microwave studio 2018.The mesh settings are shown below.

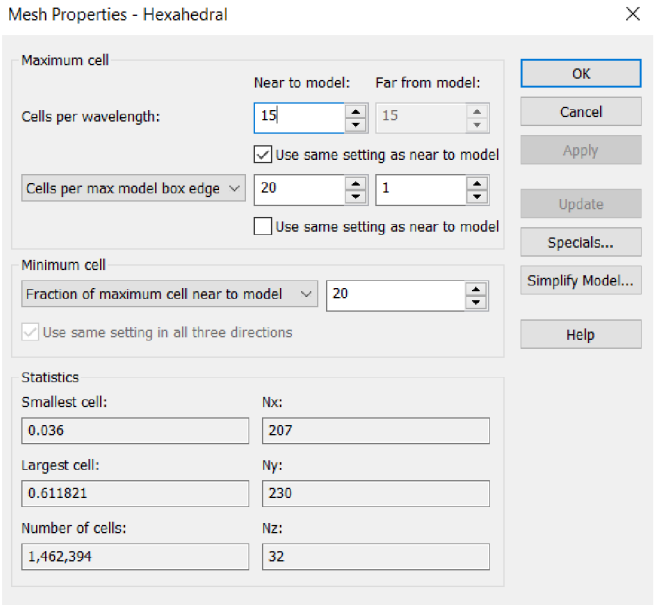

Figure 4.7 Mesh properties for the 2×2 antenna array on new substrates

Using the information from the previous sub-chapter, the essential parameters *a1, a2* and *Lt* were used in tuning the antenna reflection coefficient, axial ratio, and gain. The dimensions *a1* and *a2* were set to 7.8 mm and 8.6 mm respectively after optimization. The antenna design in CST Microwave studio is shown in the Figure 4.8.

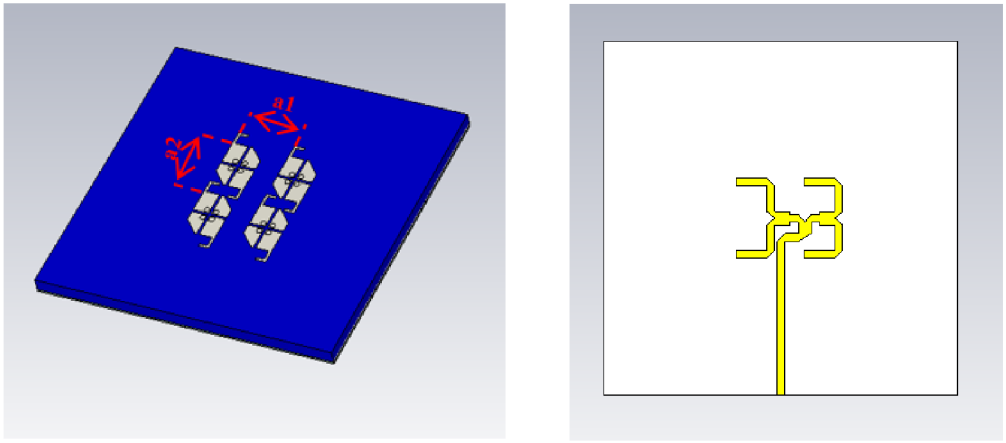

Figure 4.8 Numerical model of the 2×2 antenna array in CST Microwave Studio: (a) top view, (b) bottom view

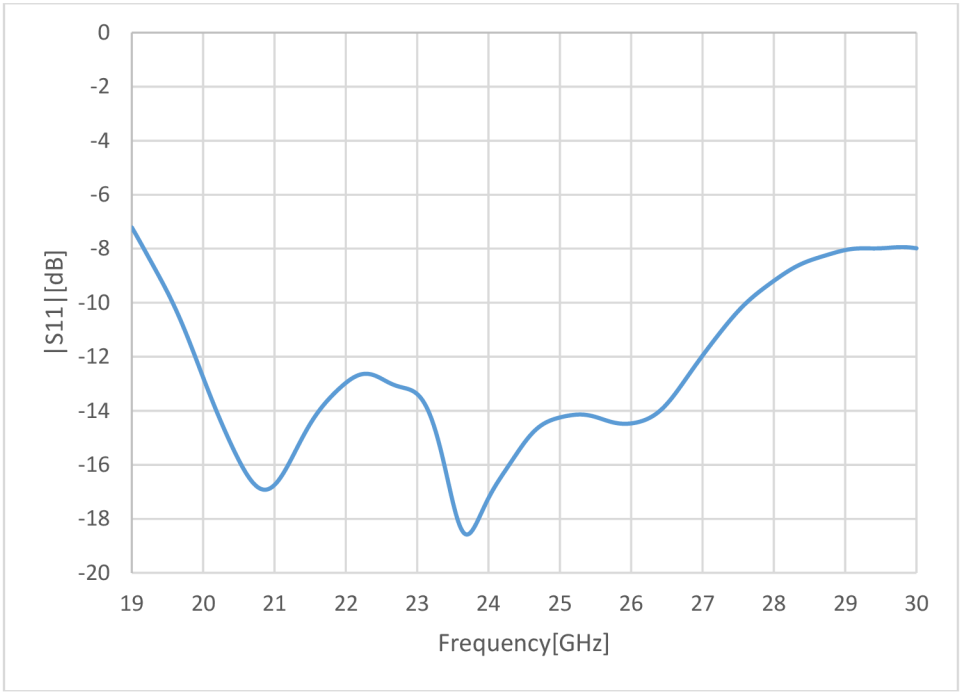

Figure 4.9 Frequency response of reflection coefficient of the 2x2 antenna array on new substrates

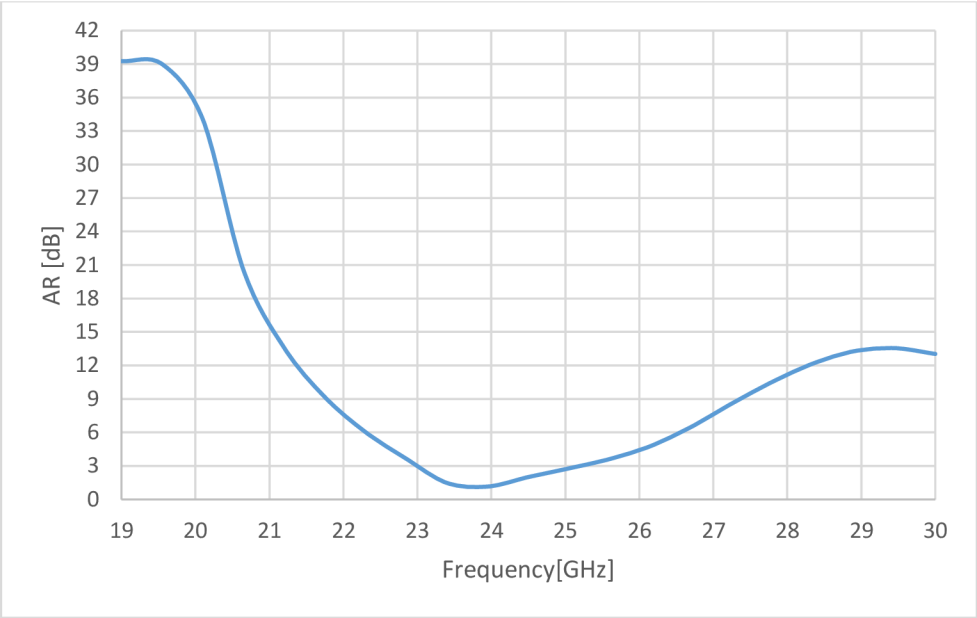

Figure 4.10 Frequency response of axial ratio of the 2x2 antenna array on new substrates

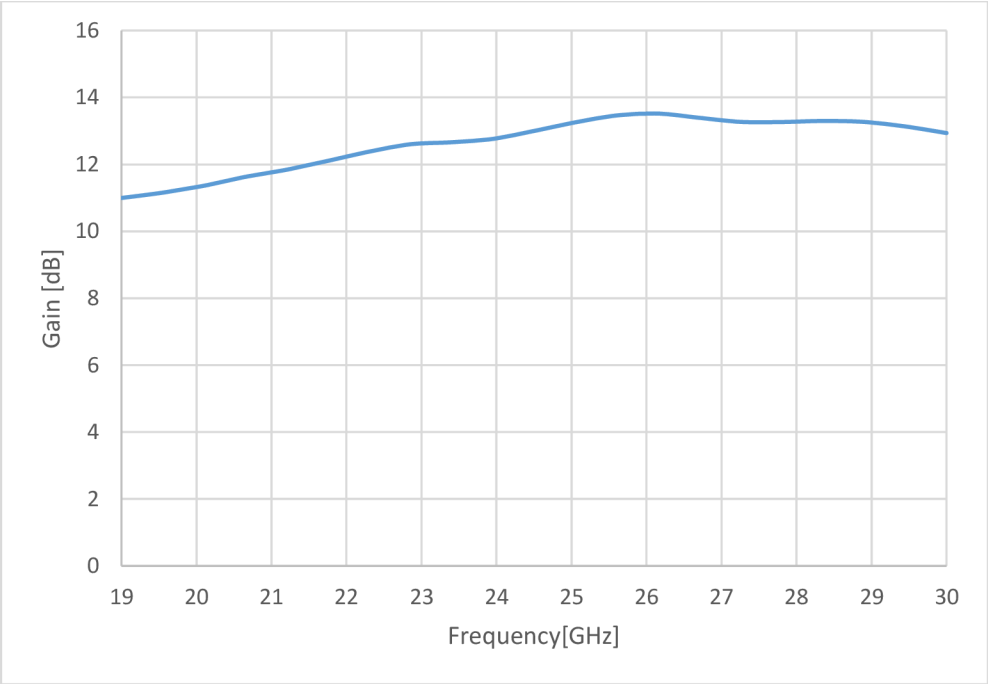

Figure 4.11 Frequency response of gain of the 2x2 antenna array on new substrates

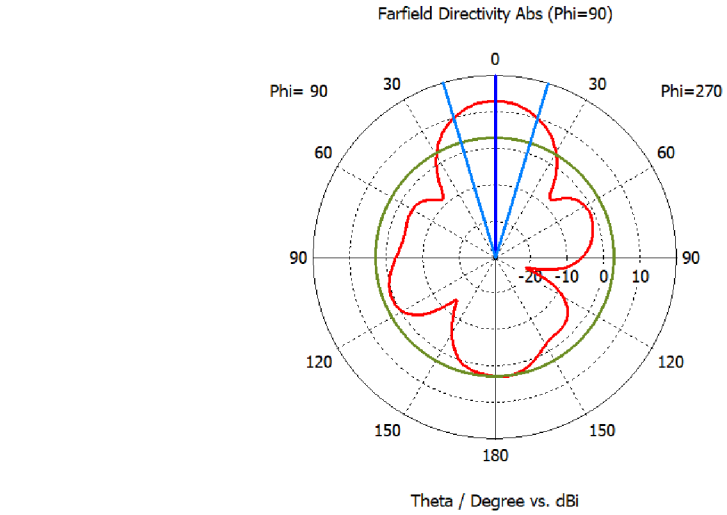

(a)

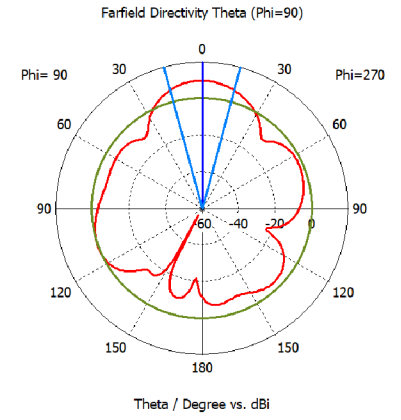

(b)

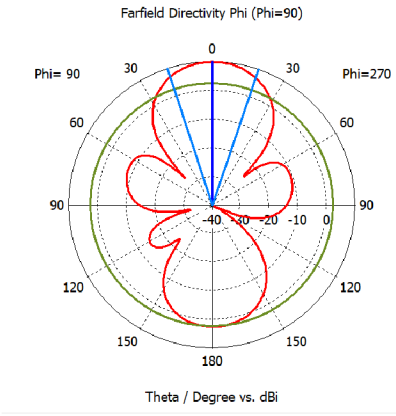

(c)

Figure 4.12 Radiation pattern of the 2x2 antenna array on new substrates: (a) Absolute radiation, (b) Theta component, (c) Phi component

Parameter	ARLON CuClad217	Rogers5880 & Rogers4003
	Value	Value
Impedance bandwidth (|S11|< -10 dB)	33.5%	24.6%
AR bandwidth (3 dB)	9.2%	Less than 1.0 %
Peak Gain	13.5 dB	13.9 dB
Minor lobe level	-10.2 dB	-16.5 dB

Table 4.3 Comparison of performance of the 2×2 antenna array design on ARLON CuClad217 substrate (available) and substrates from [1] (original substrates)

Parameter	Value [mm]
L_1	1.9
L_2	2.8
S_1	1.1
S_2	1.1
G_1	0.3
G_2	0.3
P_1	1.2
P_2	1.2
P_3	0.3
T_1	1.6
T_2	1.6
L_S	5.5
W_s	0.2
W_f	0.8
S	1.4
L	35
W	35
L_t	1.8

Table 4.4 Dimensions of the optimized 2×2 antenna array on available substrates

As can be seen from the frequency characteristics of reflection coefficient, axial ratio and gain in Figure 4.9 to Figure 4.11 respectively, the impedance bandwidth of the antenna is 33.5%, the 3 dB axial ratio bandwidth is 9.2 % and the gain is above 11 dB for frequencies from 19 GHz to 30 GHz with a peak gain of 13.5 dB.

The use of a thicker top substrate led to smaller values of the length and width of the cp antenna elements, making it possible to reduce the inter-element distances in both the x and y axes. This helped to significantly improve the antenna impedance and axial ratio bandwidths as can be seen in Table 4.4.The gain was slightly lower however, and the backward radiation was worsened.

5. NOVEL 4×4 CP ANTENNA ARRAY AT 24 GHz

A 4x4 antenna array was designed with a compact microstrip feed network as shown in Figure 5.1. The antenna elements are separated by the distance *a1* = 7.8 mm in the x-axis and the distance *a2* = 8.6 mm in the y-axis. A 2.40 mm Jack female end launch connector by Southwest Microwave was used in the model of the antenna as shown in the figure below.

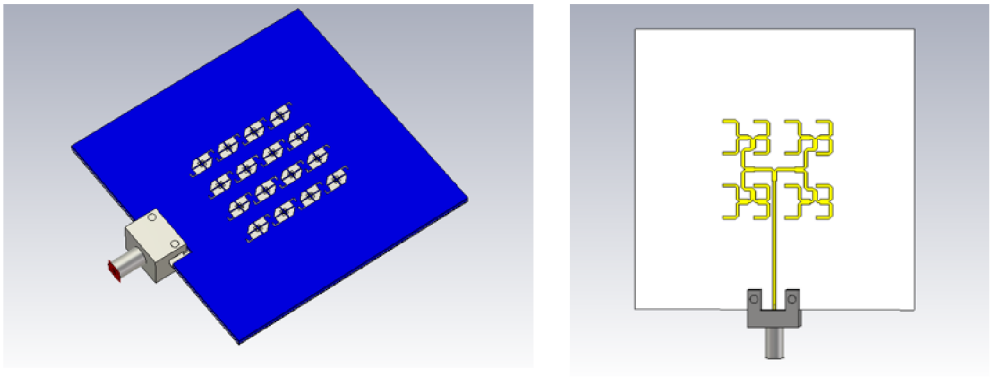

(a) **(b)**

Figure 5.1 Numerical model of the 4×4 antenna array in CST Microwave Studio: (a) top view, (b) bottom view

The optimized and simulated results of the antenna array are shown in Figure 5.2 - Figure 5.4. The impedance bandwidth is 31.6 % (from 19.17 GHz to 26.75 GHz) while the axial ratio bandwidth is 14.2 % (from 22.96 GHz to 26.37 GHz). Simulations showed that an improvement of the axial ratio bandwidth slightly worsened the impedance bandwidth, and vice-versa. A compromise was therefore made during the optimization, which led to the impedance bandwidth of the antenna array being slightly narrower than that of the 2×2 antenna array. The simulated gain was above 16.5 dB from 16.6 GHz to 30.0 GHz with a peak value of 19,0 dB.

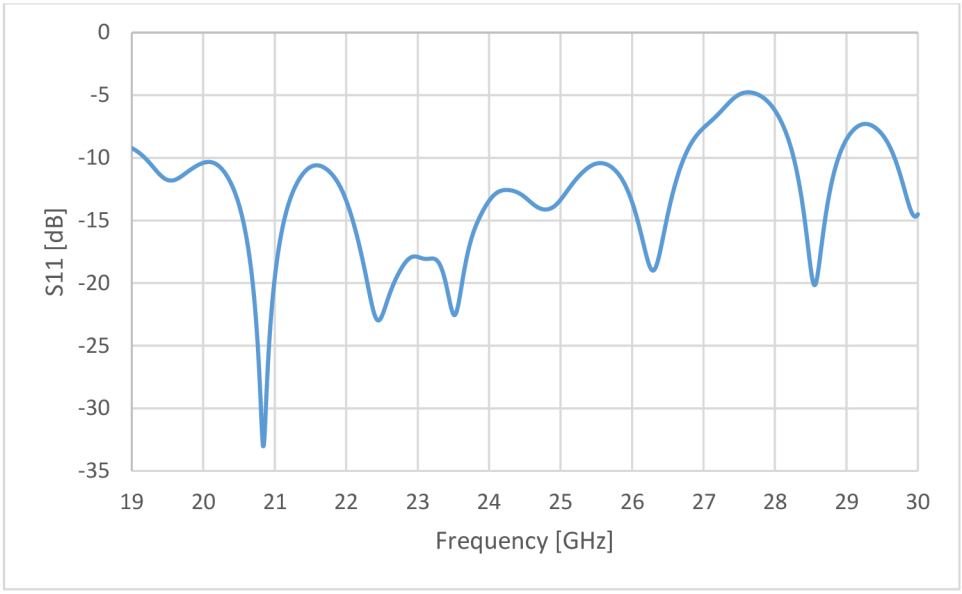

Figure 5.2 Frequency characteristic of reflection coefficient of the 4×4 antenna array on available substrates

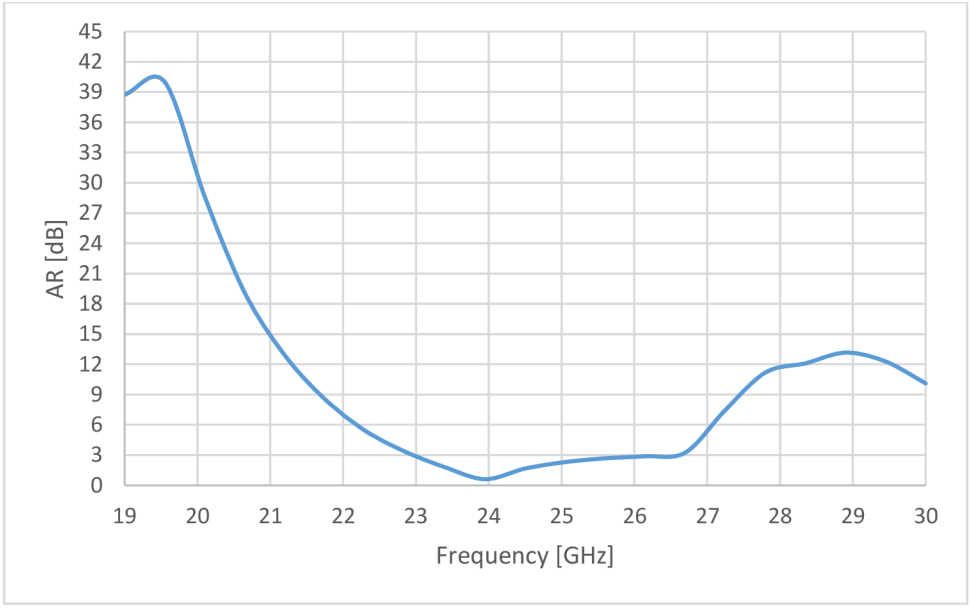

Figure 5.3 Frequency characteristic of axial ratio of the 4×4 antenna array on available substrates

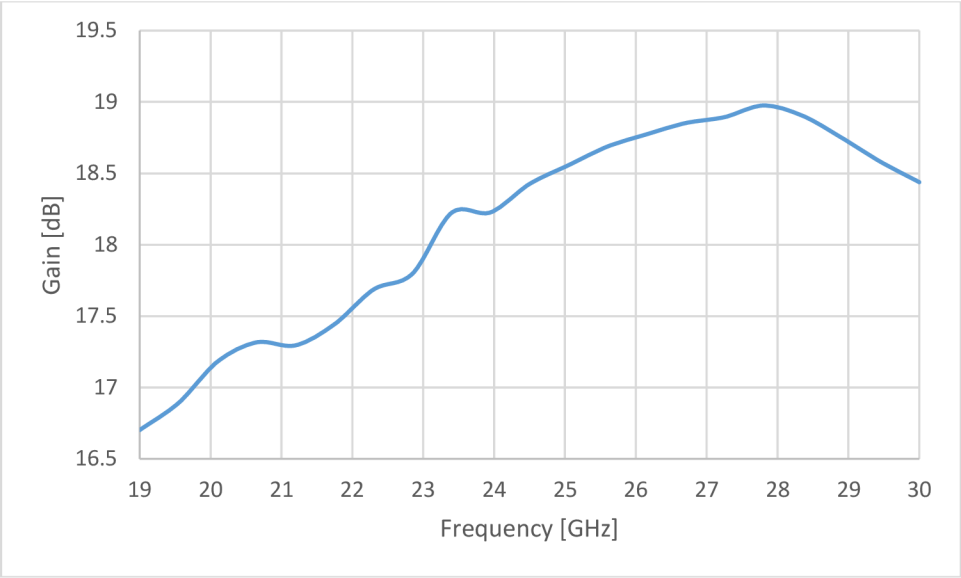

Figure 5.4 Frequency characteristic of gain of the 4×4 antenna array on available substrates

The normalized radiation pattern of the 4x4 antenna array is depicted in Figure 5.5. The side lobe level is equal to -10.5 dB and its low level (see Figure 5.5) is given with reference to the back lobe (at theta 180°) which is contributed by spurious radiation of the microstrip feed network.

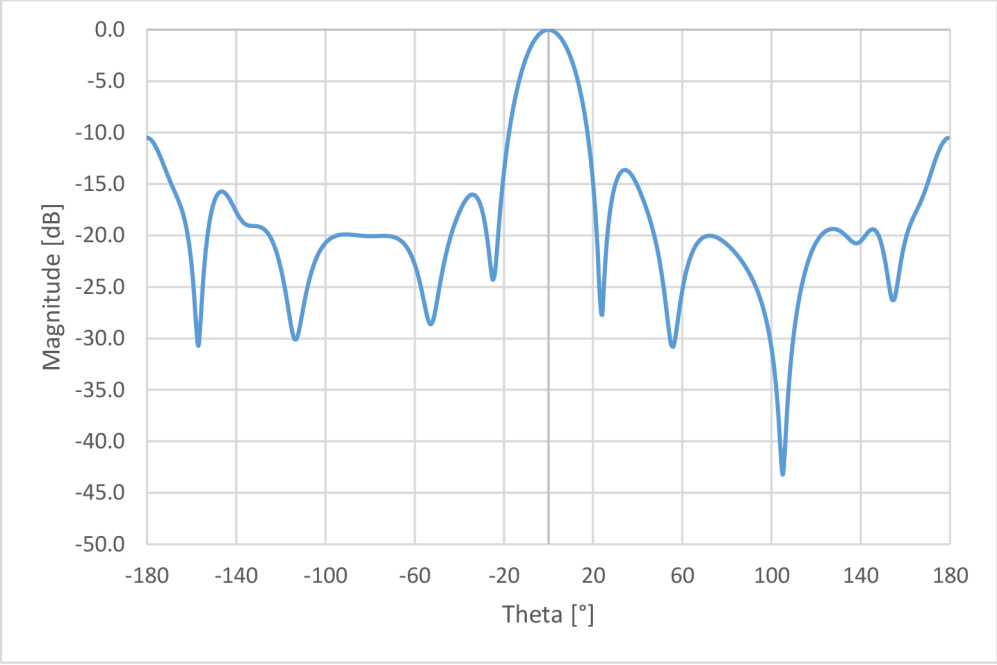

Figure 5.5 Normalized radiation pattern of the 4x4 antenna array on available substrates at 24 GHz

Parameter	Value
Bandwidth(|S11|<-10dB)	31.6 %
3dB AR Bandwidth	14.2 %
Maximum Gain	19.0 dB
Side lobe level	-10.5 dB

Table 5.1 Parameters of the optimized 4x4 antenna array on available substrates

Parameter	Value [mm]
L_1	1.9
L_2	2.8
S_1	1.1
S_2	1.1
G_1	0.3
G_2	0.3
P_1	1.2
P_2	1.2
P_3	0.3
T_1	1.6
T_2	1.6
L_S	5.5
W_s	0.2
W_f	0.8
S	1.4
L	70
W	70
L_t	1.8

Table 5.2 Dimensions of the optimized 4x4 antenna array on available substrates

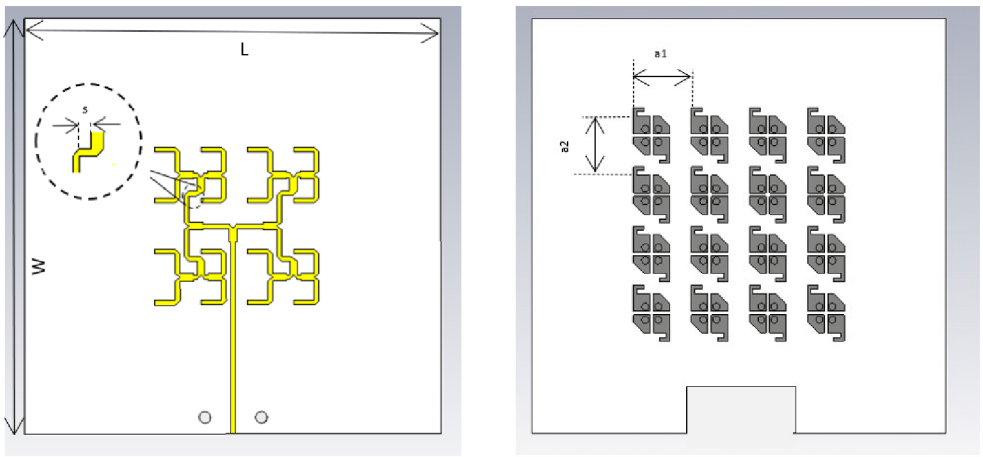

Figure 5.6 Configuration of the 4×4 antenna array on available substrates

6. CONCLUSION

A new circularly polarized antenna element that was published in the recommended literature was simulated and analyzed. The results of the analysis revealed that the antenna exhibits circular polarization mainly because of the L-shaped branches and the truncated corners. These features, however, do not only have an impact on the axial ratio but also on resonance frequency and impedance bandwidth. An increase in the level of truncations improved the axial ratio and had a very small impact on bandwidth and resonance frequency while the L-shaped branches improved axial ratio only within a small range above and below which the results worsened. Just like the L-branches, the spacing between the patches had the tendency of improving results in a small range (in this case between 0.04 and 0.30 mm). Within this range, the axial ratio increased while the reflection coefficient and impedance bandwidth improved. The results also revealed that the radius of the metallic posts connecting the patches and the ground should be small in comparison to the size of the patch and the wavelength in the dielectric and the distance between them should be kept small as well.

The results of the simulated antenna in the 45 GHz band were in absolute conformity with the results published in the recommended literature with an exception of the axial ratio which was less by 3%. Nonetheless, the overall performance of the antenna was good as it exhibited wide bandwidths for -10 dB impedance bandwidth and 3 dB AR bandwidth of 24.5% and 14.3% respectively. Comparing its performance with that of a conventional cross-aperture coupled patch antenna designed with the same substrates, its impedance and axial ratio bandwidths were about 4 and 3 times wider respectively. Due to its better performance, the novel microstrip antenna was used in the construction of the antenna array at 24 GHz.

The antenna element was used to assemble a 2×2 antenna array on the original substrates Rogers 5880 (upper substrate, $\varepsilon_r = 2.20$, h = 0.787 mm) and Rogers 4003 (lower substrate, $\varepsilon_r = 3.55$, h = 0.203 mm). The impedance bandwidth of this antenna array was 24.6%, and the maximum gain was 13.9 dB. However, the antenna array achieved an axial ratio of 3 dB only at the operating frequency of 24 GHz.

The parameters could be improved by reducing the distance between the individual elements of the array. However, this reduction was not possible due to geometrical limitations of the microstrip feeding network. Therefore, the lower substrate Rogers 4003 ($\varepsilon_r = 3.55$, h = 0.203 mm) was replaced by the substrate ARLON CuClad217 with permittivity $\varepsilon_r = 2.17$ and height h = 0.254 mm. ARLON CuClad217 with the same permittivity and height h = 1.54 mm was used as the upper substrate. The antenna array then achieved a larger impedance bandwidth of 33.5%, a larger axial ratio bandwidth of 9.2% and a maximum gain of 13.5 dB. However, the radiation pattern was deteriorated.

A 4x4 antenna array on the same available substrates was then constructed. It had a wide bandwidth of 31.6 % for $|S11| < -10$ dB in the frequency range of 19.17 GHz to 26.75 GHz and gain above 16.5 dB for a frequency range of 19 GHz to 30 GHz with a peak value of 19.0 dB. The 3 dB axial ratio bandwidth was 14.2 % for the frequency range of 22.96 GHz to 26.37 GHz and therefore sufficiently covers the whole 24 GHz ISM band (24 GHz to 24.25 GHz).The side lobe level was high however (-10.5 dB) due to spurious radiation of the microstrip feed network. The antenna design is ready for fabrication and experimental verification.

7. BIBLIOGRAPHY

[1] GAN, Zheng, Zhi-Hong TU, Ze-Ming XIE, Qing-Xin CHU a Yue YAO. Compact Wideband Circularly Polarized Microstrip Antenna Array for 45 GHz Application. *IEEE Transactions on Antennas and Propagation* [online]. 2018, **66**(11), 6388-6392 [cit. 2019-12-12]. DOI: 10.1109/TAP.2018.2863243. ISSN 0018-926X. Dostupné z: https://ieeexplore.ieee.org/document/8425689/

[2] BALANIS, Constantine A. *Antenna theory: analysis and design*. 3rd ed. Hoboken, NJ: John Wiley, c2005. ISBN isbn0-471-66782-x.

[3] KA MING MAK a KWAI MAN LUK. A Circularly Polarized Antenna with Wide Axial Ratio Beamwidth. *IEEE Transactions on Antennas and Propagation* [online]. 2009, **57**(10), 3309-3312 [cit. 2019-12-12]. DOI: 10.1109/TAP.2009.2029370. ISSN 0018-926X. Dostupné z: http://ieeexplore.ieee.org/document/5196744/

[4] YANG, Shing-Lung Steven, Ahmed A. KISHK a Kai-Fong LEE. Wideband Circularly Polarized Antenna With L-Shaped Slot. *IEEE Transactions on Antennas and Propagation* [online]. 2008, **56**(6), 1780-1783 [cit. 2019-12-12]. DOI: 10.1109/TAP.2008.923340. ISSN 0018-926X. Dostupné z: http://ieeexplore.ieee.org/document/4538175/

[5] RAIDA, Z. *Přednášky Elektromagnetické vlny, vedení a antény: Drátové a planární antény*. Dostupné také z: http://www.urel.feec.vutbr.cz/~raida/beva/lectures/BEVA_10.pdf

[6] VLASITS, T., E. KOROLKIEWICZ, A. SAMBELL a B. ROBINSON. Performance of a cross-aperture coupled single feed circularly polarised patch antenna. *Electronics Letters* [online]. 1996, **32**(7) [cit. 2019-12-12]. DOI: 10.1049/el:19960459. ISSN 00135194. Dostupné z: https://digital-library.theiet.org/content/journals/10.1049/el_19960459

[7] Intelsat Satellite telecommunications company. *Circular Polarization vs. Linear Polarization* [online]. [cit. 2019-12-12]. Dostupné z: www.intelsat.com/wp-content/uploads/2013/02/Polarization.pdf

[8] RAINA, Tanveer Kour, Amanpreet KAUR a Rajesh KHANNA. Design of Aperture Coupled Micro-Strip Patch Antenna for Wireless Communication Applications at 10Ghz (X BAND. *International Journal of Electronics Engineering*. Serials Publications, 2012, **4**(1), 25-28. ISSN 0973-7383.

[9] NDUJIUBA, Charles U., Adebiyi A. ADELAKUN a Oboyerulu E AGBOJE. Hybrid Method of Analysis for Aperture-Coupled Patch Antenna Array for MIMO Systems. *International Journal of Electromagnetics and Applications*. 2015, **5**(2), 90-97. DOI: 10.5923/j.ijea.20150502.03. ISSN 2168-5045.

[10] DASSAULT SYSTÈMES. *CST STUDIO SUITE ™ 2006: Tutorials* [online]. 2005 [cit. 2020-05-27]. Dostupné z: https://perso.telecom-paristech.fr/begaud/intra/MWS_Tutorials.pdf

[11] DASSAULT SYSTÈMES. *Understanding Time Domain Meshing in CST MICROWAVE STUDIO®* [online]. 2010 [cit. 2020-05-27]. Dostupné z: https://www.researchgate.net/file.PostFileLoader.html?id=578c450ceeae3937441b63a1&assetKey=AS%3A385033333428224%401468810508239